

# SCIENTIFIC REPORTS

OPEN

## Expression of plasma membrane calcium ATPases confers $\text{Ca}^{2+}/\text{H}^{+}$ exchange in rodent synaptic vesicles

Yoshiyasu Ono<sup>1</sup>, Yasunori Mori<sup>1</sup>, Yoshihiro Egashira<sup>1,3</sup>, Kenta Sumiyama<sup>2</sup> & Shigeo Takamori<sup>1</sup>

$\text{Ca}^{2+}$  transport into synaptic vesicles (SVs) at the presynaptic terminals has been proposed to be an important process for regulating presynaptic  $[\text{Ca}^{2+}]$  during stimulation as well as at rest. However, the molecular identity of the transport system remains elusive. Previous studies have demonstrated that isolated SVs exhibit two distinct  $\text{Ca}^{2+}$  transport systems depending on extra-vesicular (cytosolic) pH; one is mediated by a high affinity  $\text{Ca}^{2+}$  transporter which is active at neutral pH and the other is mediated by a low affinity  $\text{Ca}^{2+}/\text{H}^{+}$  antiporter which is maximally active at alkaline pH of 8.5. In addition, synaptic vesicle glycoprotein 2 s (SV2s), a major SV component, have been proposed to contribute to  $\text{Ca}^{2+}$  clearance from the presynaptic cytoplasm. Here, we show that at physiological pH, the plasma membrane  $\text{Ca}^{2+}$  ATPases (PMCAs) are responsible for both the  $\text{Ca}^{2+}/\text{H}^{+}$  exchange activity and  $\text{Ca}^{2+}$  uptake into SVs. The  $\text{Ca}^{2+}/\text{H}^{+}$  exchange activity monitored by acidification assay exhibited high affinity for  $\text{Ca}^{2+}$  ( $K_m \sim 400 \text{ nM}$ ) and characteristic divalent cation selectivity for the PMCAs. Both activities were remarkably reduced by PMCA blockers, but not by a blocker of the ATPase that transfers  $\text{Ca}^{2+}$  from the cytosol to the lumen of sarcoplasmic endoplasmic reticulum (SERCA) at physiological pH. Furthermore, we rule out the contribution of SV2s, putative  $\text{Ca}^{2+}$  transporters on SVs, since both  $\text{Ca}^{2+}/\text{H}^{+}$  exchange activity and  $\text{Ca}^{2+}$  transport were unaffected in isolated vesicles derived from SV2-deficient brains. Finally, using a PMCA1-pHluorin construct that enabled us to monitor cellular distribution and recycling properties in living neurons, we demonstrated that PMCA1-pHluorin localized to intracellular acidic compartments and recycled at presynaptic terminals in an activity-dependent manner. Collectively, our results imply that vesicular PMCAs may play pivotal roles in both presynaptic  $\text{Ca}^{2+}$  homeostasis and the modulation of  $\text{H}^{+}$  gradient in SVs.

Synaptic vesicles (SV) are storage organelles for neurotransmitters and play a key role in synaptic transmission. Vesicular transport of classical neurotransmitters including glutamate, GABA/glycine, biogenic monoamines, acetylcholine, and adenosine triphosphate (ATP) is mediated by the respective vesicular transporters for these neurotransmitters. Vesicular transport is driven by a proton electrochemical gradient generated by the vacuolar-type  $\text{H}^{+}$  ATPase (V-ATPase)<sup>1</sup>. The V-ATPase generates both a pH gradient ( $\Delta\text{pH}$ ) and a membrane potential (internal positive voltage,  $\Delta\Psi$ ) across the SV membrane. Depending on the chemical properties of neurotransmitters and the intrinsic characteristics of vesicular transporters, the dependence of neurotransmitter uptake on either driving force varies among the neurotransmitters. In principle, the uptake of cationic transmitters such as monoamines and acetylcholine depends primarily on  $\Delta\text{pH}$ , whereas the uptake of anionic transmitters such as glutamate and ATP depends more on  $\Delta\Psi$ , although pivotal roles of protons in glutamate transport have also been suggested<sup>2–4</sup>. The uptake of zwitter-ionic transmitters such as GABA and glycine depends equally on both  $\Delta\text{pH}$  and  $\Delta\Psi$  (but see Juge *et al.*<sup>5</sup> who proposed a predominant role of  $\Delta\Psi$ ). Therefore, a balance between  $\Delta\text{pH}$  and  $\Delta\Psi$  across individual SVs differentially regulate transport rates and storage of neurotransmitters in SVs<sup>1</sup>.

<sup>1</sup>Laboratory of Neural Membrane Biology, Graduate School of Brain Science, Doshisha University, 1-3 Tatara-Miyakodani, Kyotanabe, Kyoto, 610-0394, Japan. <sup>2</sup>Laboratory for Mouse Genetic Engineering, RIKEN Center for Biosystems Dynamics Research, 1-3 Yamadaoka, Suita, Osaka, 565-0871, Japan. <sup>3</sup>Present address: Department of Physiology, Faculty of Medicine, Osaka Medical College, 2-7 Daigaku-machi, Takatsuki, Osaka, 569-8686, Japan. Correspondence and requests for materials should be addressed to S.T. (email: [stakamor@mail.doshisha.ac.jp](mailto:stakamor@mail.doshisha.ac.jp))

The balance between  $\Delta\text{pH}$  and  $\Delta\Psi$  is regulated by the permeability of the SV membrane to various charged ions and their concentration gradients<sup>6</sup>. In fact, SVs contain various transporters and/or channels for ions that directly or indirectly modulate  $\text{H}^+$  flux across SVs. For instance, it has been demonstrated that SVs exhibit a  $\text{Cl}^-$  conductance that serves a shunting current for  $\text{H}^+$ , resulting in an increase in net proton influx and thus a generation of larger  $\Delta\text{pH}$ <sup>7,8</sup>. In the case of SVs that store glutamate, the vesicular glutamate transporters (VGLUTs) are proposed to confer the  $\text{Cl}^-$  flux<sup>2,3,9,10</sup> (but see also Juge *et al.*<sup>11</sup>). The contribution of the chloride channel (CLC) family has been proposed, especially for SVs that transport other neurotransmitters, but their physiological relevance remains controversial<sup>12–15</sup>. More recently, cation/ $\text{H}^+$  exchange activity conferred by either  $\text{Na}^+/\text{H}^+$  exchangers (NHEs)<sup>16</sup> or VGLUTs<sup>10</sup> (in the case of glutamate-containing vesicles) were shown to decrease  $\Delta\text{pH}$  and consequently facilitate  $\Delta\Psi$ . In stark contrast, the contribution of divalent cations such as  $\text{Ca}^{2+}$  and  $\text{Zn}^{2+}$  has received less attention. To date, the mechanism and molecular entity of the transporting molecule(s) remain elusive.

Classical studies using SV fraction isolated from the electric organ of *Torpedo marmorata* revealed that SVs exhibited an ATP-dependent active  $\text{Ca}^{2+}$  transport activity<sup>17–19</sup>. Consistent with this, a transient increase of  $\text{Ca}^{2+}$  in the SV lumen was observed after stimulation at the cholinergic synapses of the electric organ of *Torpedo marmorata*<sup>20</sup>, suggesting that SVs can function as a  $\text{Ca}^{2+}$  store at presynaptic terminals in a physiological context. Efforts to decipher the  $\text{Ca}^{2+}$  transport protein(s) in mammalian SVs have revealed that at least two distinct mechanisms may exist: vanadate-sensitive P-type Calcium ATPases, which are fully active at neutral pH, and a molecularly unidentified  $\text{Ca}^{2+}/\text{H}^+$  antiporter, which functions maximally at alkaline pH of 8.5<sup>21–23</sup>. These two transport systems exhibit substantial differences in their affinities for  $\text{Ca}^{2+}$ . While  $K_m$  of the vanadate-sensitive  $\text{Ca}^{2+}$  ATPases lies in the order of several hundred nM,  $K_m$  of the  $\text{Ca}^{2+}/\text{H}^+$  antiporter exceeds 300  $\mu\text{M}$ , which far surpasses physiological  $\text{Ca}^{2+}$  concentrations at presynaptic terminals<sup>24</sup>. Moreover, these two transport systems exhibit characteristic dependence on  $\text{Ca}^{2+}$  concentrations. Notably,  $\text{Ca}^{2+}$  ATPase activity increases with  $\text{Ca}^{2+}$  concentration in the medium, reaching a maximum at  $\sim 25 \mu\text{M}$ , whereas its activity is inhibited at higher  $\text{Ca}^{2+}$  concentrations and is completely abolished at  $\sim 500 \mu\text{M}$   $\text{Ca}^{2+}$ <sup>22</sup>.

Aside from these two SV  $\text{Ca}^{2+}$  transport systems, it has long been conjectured that one of the major SV proteins, SV2s (synaptic vesicle glycoprotein 2s), may function as a  $\text{Ca}^{2+}$  transporter in SVs<sup>25</sup>, because the genetic deletion of SV2s revealed synaptic phenotypes that could be well-explained by the increase in cytoplasmic  $[\text{Ca}^{2+}]$ <sup>26,27</sup> (but see<sup>28</sup>). Nevertheless, the relative contributions of these proteins to  $\text{Ca}^{2+}$  transport into SVs has not been elucidated, and whether/how the activities of these proteins may affect  $\Delta\mu\text{H}^+$  to influence neurotransmitter uptake remains unclear.

In this study, we aimed to clarify the molecular identity of the  $\text{Ca}^{2+}$  transporting protein(s) in SVs and how their activity influences  $\Delta\mu\text{H}^+$  of SVs. Using a fast  $\text{Ca}^{2+}$  chelator BAPTA, instead of EGTA that was previously used to control free  $\text{Ca}^{2+}$  concentrations in the buffer<sup>21,29</sup>, we show that SVs isolated from rodent brains exhibit high affinity  $\text{Ca}^{2+}/\text{H}^+$  exchange activity even at neutral pH that would attenuate  $\Delta\text{pH}$  in SVs. Biochemical properties of the exchanger such as the affinity for  $\text{Ca}^{2+}$ , ion selectivity, and sensitivity to specific inhibitors resemble those of the plasma membrane  $\text{Ca}^{2+}$  ATPases (PMCA). Furthermore, we ruled out a contribution of SV2s to  $\text{Ca}^{2+}$  uptake into SVs by analyzing vesicle fractions from SV2-deficient brains. We further demonstrated using a pH-sensitive fluorescent protein (pHluorin)<sup>30</sup> as a reporter that PMCA1, an isoform of PMCA expressed in the mammalian nervous system, indeed resides mainly on SVs and is capable of recycling at presynaptic terminals in an activity-dependent manner. Given the predominant role of PMCA in regulating  $\text{Ca}^{2+}$  homeostasis at presynaptic terminals<sup>31</sup>, our results imply that vesicular PMCA play dual roles at presynaptic terminals in  $\text{Ca}^{2+}$  homeostasis and in modulating  $\Delta\mu\text{H}^+$  in SVs via  $\text{Ca}^{2+}/\text{H}^+$  antiport activity.

## Results

**A  $\text{Ca}^{2+}/\text{H}^+$  exchanger in SVs operates at neutral pH.** Evidence that SVs isolated from sheep brain cortex contain low affinity  $\text{Ca}^{2+}/\text{H}^+$  antiport activity relied essentially on an acidification assay in which fluorescence quenching of acridine orange due to V-ATPase-dependent acidification was reversed by addition of  $\text{Ca}^{2+}$ <sup>21–23</sup>. This activity was characterized by its low affinity ( $K_m > 200 \mu\text{M}$ ) and operated at pH 8.5. However, chelation of  $\text{Ca}^{2+}$  by EGTA would result in rapid liberation of  $\text{H}^+$  from EGTA, and the ability of  $\text{Ca}^{2+}$  chelation by EGTA depends critically on pH. As such, addition of  $\text{Ca}^{2+}$  in the presence of EGTA during the measurement may have caused a change in pH, raising the possibility that the affinity and pH dependence may have been disturbed. Therefore, we decided to use BAPTA whose  $K_D$  is similar to that of EGTA, but the ability to chelate  $\text{Ca}^{2+}$  is much less affected by pH changes. First, we tested the effect of  $\text{Ca}^{2+}$  in the presence of BAPTA at neutral pH of 7.2, and compared with that in the presence of EGTA (Fig. 1a). Acidification of crude SV fraction (LP2) was induced by adding 2 mM ATP in the presence of 100 mM  $\text{Cl}^-$ , and 600  $\mu\text{M}$   $\text{Ca}^{2+}$  was then added. As observed in previous studies at pH 8.5<sup>21,23</sup>, slow alkalization of SVs was also observed in the presence of EGTA (Fig. 1a, red trace in the left panel). Notably, the effect of  $\text{Ca}^{2+}$  was more pronounced when the assay was performed in the presence of BAPTA (Fig. 1a, red trace in the right panel), indicating that the  $\text{Ca}^{2+}/\text{H}^+$  exchange activity was also operative at neutral pH. Essentially, the same results were obtained under conditions where acidification was monitored in SVs pre-acidified by VGLUT-mediated glutamate transport<sup>3</sup> (Fig. 1b), confirming that the activity originated from SVs rather than contaminating organelles such as microsomes and mitochondria. To further confirm if the de-quenching represented a transporter-mediated process, we measured de-quenching velocities upon the addition of  $\text{Ca}^{2+}$  at various temperatures (32.3 °C and 37.3 °C) under the same conditions as those in Fig. 1b (right panel). The temperature co-efficient ( $Q_{10}$ ) was estimated to be  $\sim 1.6$  (Fig. 1c), which is within the range of physical properties of transporter-mediated processes rather than simple diffusion<sup>32,33</sup>.

**The vesicular  $\text{Ca}^{2+}/\text{H}^+$  exchanger exhibits high affinity for  $\text{Ca}^{2+}$ .** To estimate the affinity of the  $\text{Ca}^{2+}/\text{H}^+$  exchanger in SVs at neutral pH, we measured alkalization of pre-acidified SVs by various concentrations of  $\text{CaCl}_2$  in the presence of a fixed concentration of BAPTA (50  $\mu\text{M}$ ). To this end, we first estimated free  $\text{Ca}^{2+}$  concentrations

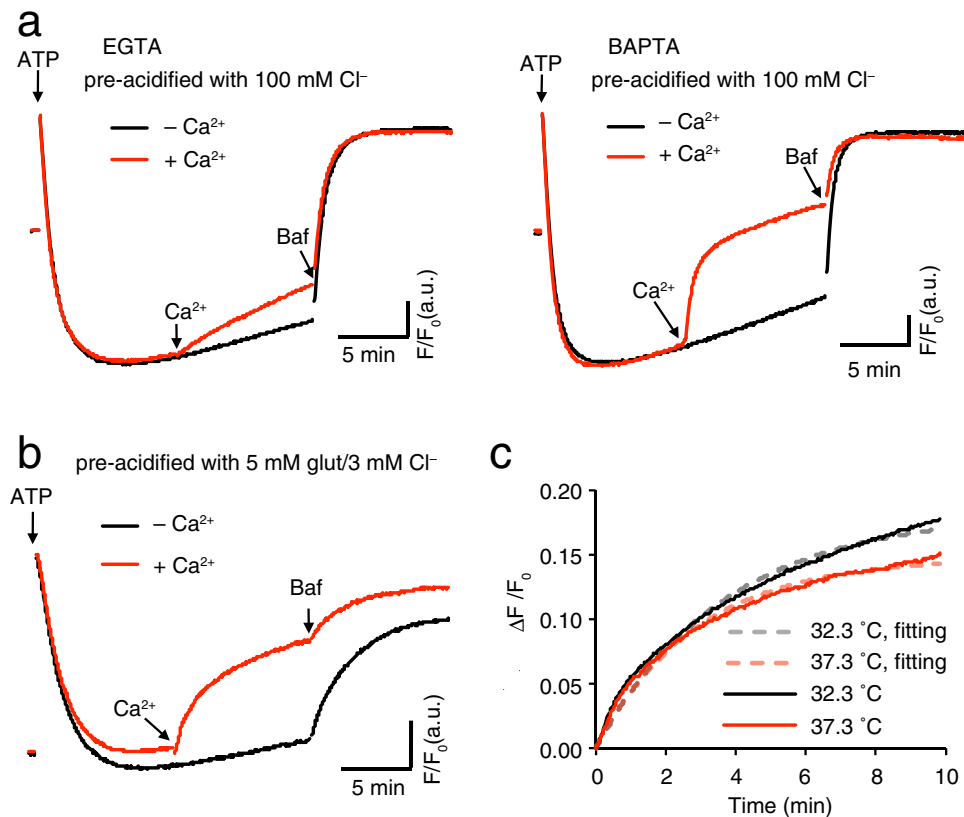


**Figure 1.**  $\text{Ca}^{2+}/\text{H}^{+}$  exchange activity attenuates  $\Delta\text{pH}$  in synaptic vesicles at neutral pH. (a) Effect of  $\text{Ca}^{2+}$  in the presence of EGTA (left) or BAPTA (right) on ATP-dependent acidification at pH 7.2. Acidification was measured using acridine orange as a reporter dye. Crude SV fraction (LP2) was incubated in the presence of 50  $\mu\text{M}$  EGTA or 50  $\mu\text{M}$  BAPTA in the presence of 100 mM KCl. To initiate acidification, 2 mM ATP was added, and 600  $\mu\text{M}$   $\text{CaCl}_2$  (only for red traces) and 500 nM Bafilomycin (Baf) were added at time points indicated by arrows. Note that de-quenching (indicated by increases in fluorescence) upon the addition of  $\text{CaCl}_2$  was greater in the presence of BAPTA than EGTA. The traces were the representative traces from more than three measurements. (b) Effect of  $\text{Ca}^{2+}$  in the presence of BAPTA on ATP-dependent, glutamate-induced acidification at pH 7.2. Crude SV fraction (LP2) was incubated in the presence of 50  $\mu\text{M}$  BAPTA in the presence of 5 mM glutamate and 3 mM KCl. To initiate acidification, 2 mM ATP was added, and 600  $\mu\text{M}$   $\text{CaCl}_2$  (only for red traces) and 500 nM bafilomycin (Baf) were added at time points indicated by arrows. The traces were the representative traces from more than three measurements. (c) Temperature coefficient ( $Q_{10}$ ) of  $\text{Ca}^{2+}$ -induced alkalization.  $\text{Ca}^{2+}$ -induced alkalization of SVs that were pre-acidified in the presence of 100 mM KCl was monitored either at 32.3 °C (black) or at 37.3 °C (red). The alkalization kinetics were obtained by exponential fittings shown in dotted lines.  $Q_{10}$  was calculated as described in Materials and Methods.

in our assay buffers using fura-2 as a  $\text{Ca}^{2+}$  indicator and found it to be  $\sim 1 \mu\text{M}$  (Supplementary Fig. 1). Taking this into account, free  $\text{Ca}^{2+}$  concentrations in the assay buffer were set by adding  $\text{CaCl}_2$  (see Materials and Methods for details). After complete acidification of SVs in the presence of 100 mM KCl was achieved, we added a series of  $\text{Ca}^{2+}$  concentrations ranging from 0 to 75  $\mu\text{M}$  that were equivalent to 3.63 to 6410 nM free  $[\text{Ca}^{2+}]$  in the assay medium. With the ranges of  $\text{Ca}^{2+}$  added, the rate of alkalization increased as a function of free  $\text{Ca}^{2+}$  concentrations (Fig. 2a). A plot of initial velocities of alkalization as a function of free  $\text{Ca}^{2+}$  concentrations revealed that  $K_m$  of  $\text{Ca}^{2+}$ -induced SV alkalization was  $\sim 400$  nM (Fig. 2b), a value that appeared to be several magnitudes lower than that reported previously<sup>21</sup>. To further characterize the  $\text{Ca}^{2+}/\text{H}^{+}$  antiport activity at neutral pH, we tested a series of divalent cations for the ability to alkalinize pre-acidified SVs. Previous studies demonstrated that, at alkaline pH,  $\text{Zn}^{2+}$  and  $\text{Cd}^{2+}$  are substrates of the same  $\text{Ca}^{2+}/\text{H}^{+}$  exchanger, whilst  $\text{Ba}^{2+}$  and  $\text{Sr}^{2+}$  are not<sup>29</sup>. In our assay conditions in the presence of BAPTA at pH 7.2,  $\text{Zn}^{2+}$  and  $\text{Cd}^{2+}$  induced alkalization of pre-acidified SVs in the presence of 100 mM KCl to a similar extent as that of  $\text{Ca}^{2+}$ , whereas  $\text{Ba}^{2+}$  induced slower but significant alkalization (Fig. 3). Consistent with previous results,  $\text{Sr}^{2+}$  showed marginal alkalization, indicating that the  $\text{Ca}^{2+}/\text{H}^{+}$  exchanger in SVs shows substrate preference as follows:  $\text{Ca}^{2+} \approx \text{Zn}^{2+} \approx \text{Cd}^{2+} > \text{Ba}^{2+} \gg \text{Sr}^{2+}$ . The same trend was observed when LP2 was pre-acidified by glutamate, indicating that the alkalization by divalent cations originated from VGLUT-containing SVs (Supplementary Fig. 2). It should be noted here that it remains unknown if these divalent cations are transported by distinct transporters with similar proton coupling, or if the alkalization resulted from the blockade of the V-ATPase activity (see also Supplementary Fig. 4 related to Fig. 5).

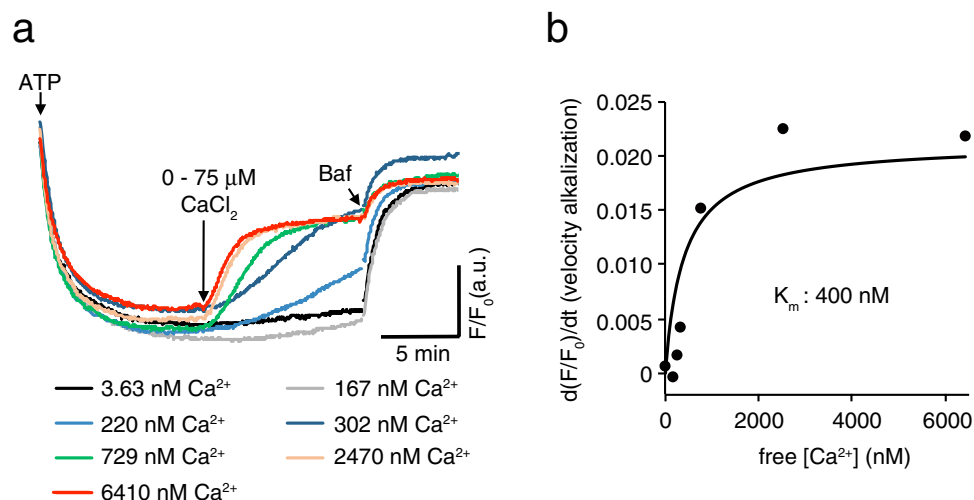


**Figure 2.** Apparent affinity of the Ca<sup>2+</sup>/H<sup>+</sup> exchanger on SVs. **(a)** Alkalization of SVs by various concentrations of Ca<sup>2+</sup>. After SVs were maximally acidified in the presence of 100 mM KCl, various concentrations of CaCl<sub>2</sub> were added. Individual traces in the presence of various free [Ca<sup>2+</sup>], ranging from 3.63–6410 nM of free [Ca<sup>2+</sup>] were color-coded. **(b)** The initial slopes of alkalization in **(a)** were plotted against free [Ca<sup>2+</sup>]. Data points were fitted with the Michaelis-Menten equation to calculate K<sub>m</sub>.

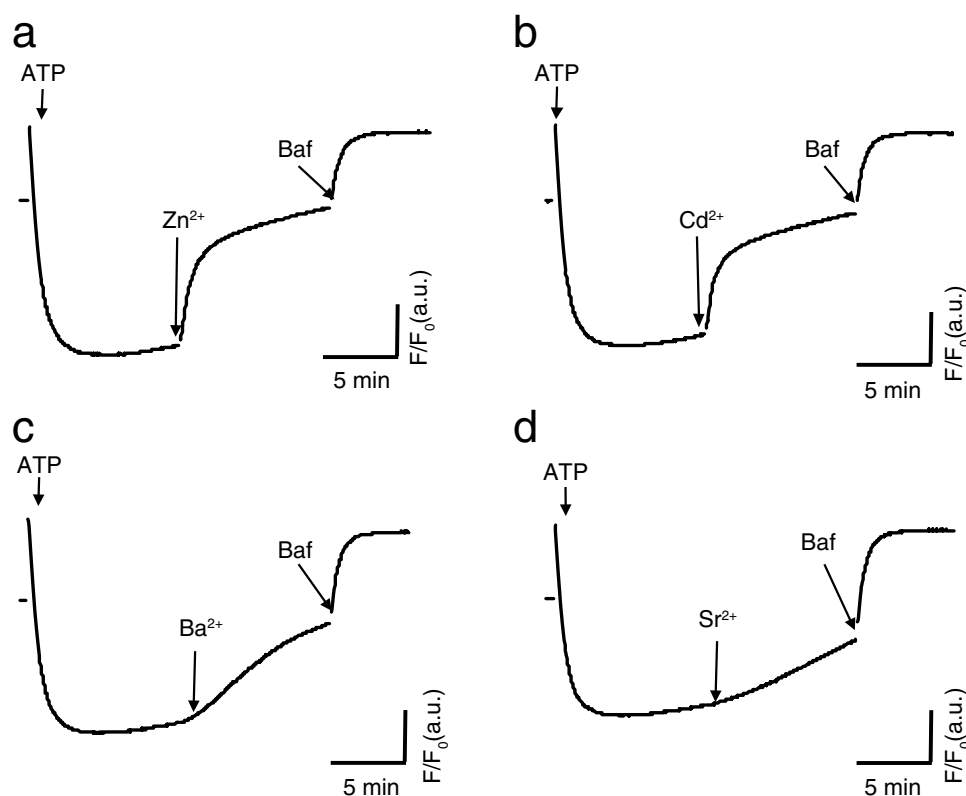


**Figure 3.** Selectivity of the Ca<sup>2+</sup>/H<sup>+</sup> exchanger for other divalent cations. LP2 fraction was acidified in the presence of 100 mM KCl at pH 7.2. After stable baselines were achieved, various divalent cations including Zn<sup>2+</sup>, Cd<sup>2+</sup>, Ba<sup>2+</sup>, and Sr<sup>2+</sup> at final concentration of 50 μM were added. The traces were the representative traces from more than three measurements. Note that we observed the same results when vesicles were pre-acidified in the presence of 5 mM glutamate and 3 mM KCl (see Supplementary Fig. 2).

**SV2s are not responsible for Ca<sup>2+</sup>/H<sup>+</sup> exchange in SVs.** As described in the Introduction, there are several candidates responsible for Ca<sup>2+</sup> transport in SVs. Comprehensive proteomic analysis of purified SV fraction identified two P-type ATPases, PMCA and one that exchanges Ca<sup>2+</sup> from the cytosol with protons in

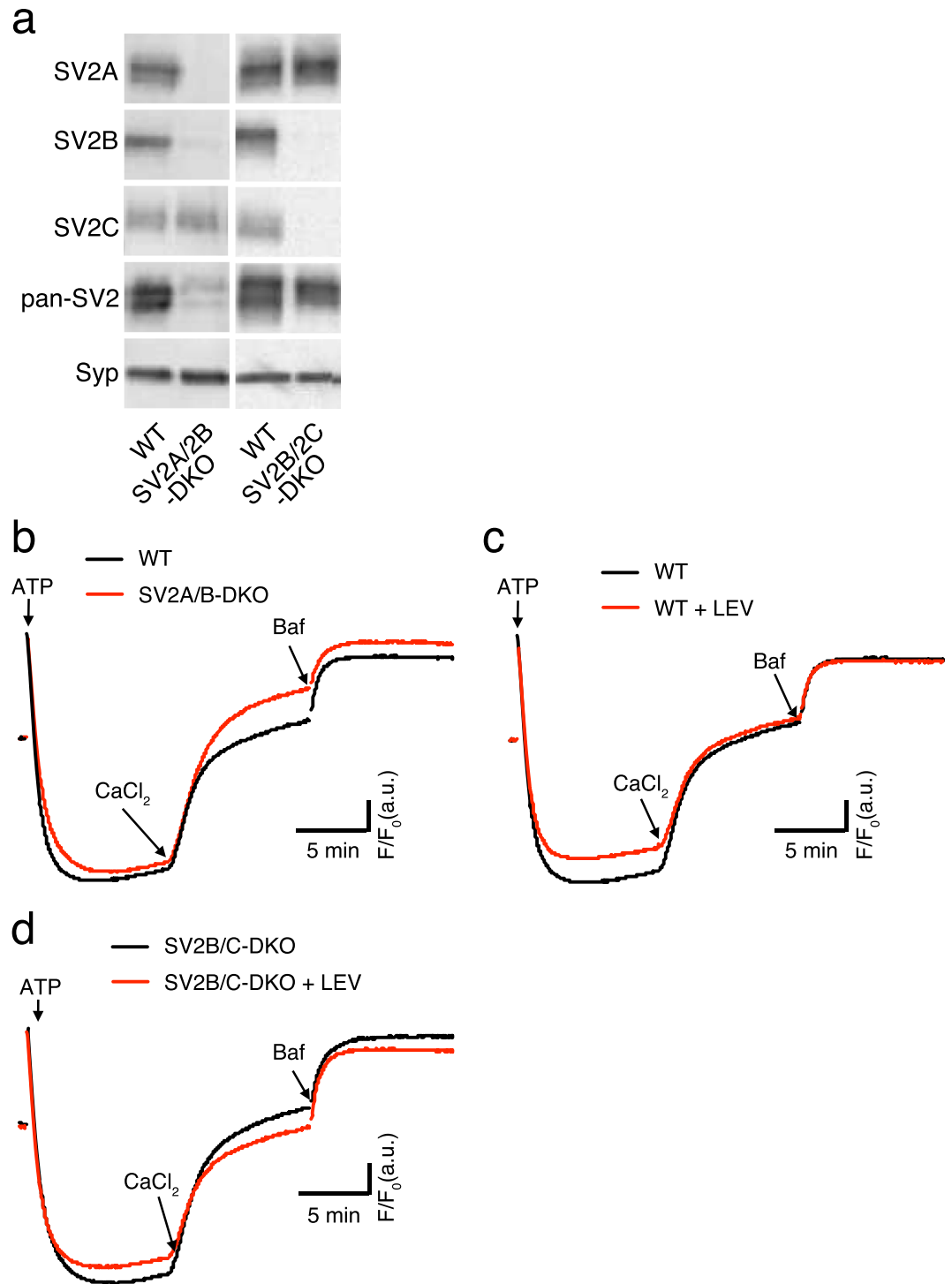


**Figure 4.** SV2s do not confer Ca<sup>2+</sup>/H<sup>+</sup> exchange. **(a)** Expression of SV2 isoforms in synaptic vesicles derived from SV2A/B-DKO and SV2B/C-DKO mice. Equal amounts of vesicle proteins from each genotype (20 μg/lane) were analyzed by western blotting using isoform-specific antibodies. Antibodies used for western blots are indicated at the left of the images. Rabbit polyclonal antibodies against SV2A, SV2B, and SV2C, and a mouse monoclonal antibody that recognizes all SV2 isoforms (pan-SV2) were used. For loading controls, a mouse monoclonal antibody against synaptophysin (Syp) (Cl7.2) was used. Note that expression of the SV2 isoforms was completely abolished in the respective DKO samples. A faint band revealed by the pan-SV2 antibody in the SV2A/2B-DKO sample indicated that SV2C content was much less than that of SV2A or SV2B. The images were cropped from four independent blots for presentation, and the original digital images of the full-length blots are presented in Supplementary Fig. 3. **(b)** Ca<sup>2+</sup>-induced alkalinization in vesicles derived from SV2A/B-DKO (red) compared to wild-type mice (black). 50 μM CaCl<sub>2</sub> was added after vesicles were pre-acidified in the presence of 100 mM KCl. **(c)** Effect of levetiracetam (LEV, 30 μM) on Ca<sup>2+</sup>-induced alkalinization in vesicles from wild-type mice. Vesicles were pre-acidified in the presence of 100 mM KCl, and 50 μM CaCl<sub>2</sub> was then added. LEV pre-

treatment (red traces) shows little impact on alkalization by  $\text{Ca}^{2+}$  compared to the respective controls without LEV pre-treatment (black traces). **(d)** Effect of levetiracetam (LEV, 30  $\mu\text{M}$ ) on  $\text{Ca}^{2+}$ -induced alkalization in vesicles from SV2B/2C-DKO mice. Measurements were performed as in **(c)**. LEV pre-treatment (red traces) shows little impact on alkalization by  $\text{Ca}^{2+}$  compared to the respective controls without LEV pre-treatment (black traces). Traces in **(b–d)** are the representative data from two to three measurements in each condition.

th elumen of sarcoplasmic endoplasmic reticulum (SERCA)<sup>34</sup>. However, contributions of these ATPases to SV acidity due to a  $\text{H}^+$  coupling have not been directly investigated. Furthermore, according to synaptic phenotypes related to changes in presynaptic  $\text{Ca}^{2+}$  concentrations and in presynaptic calcium buffering in SV2-deficient neurons<sup>26,27</sup>, it has been hypothesized that SV2s may be involved in  $\text{Ca}^{2+}$  transport into SVs. We therefore sought to clarify which protein was responsible for the observed  $\text{Ca}^{2+}/\text{H}^+$  exchange activity in SVs at neutral pH.

First, in order to verify the contribution of SV2s in  $\text{Ca}^{2+}/\text{H}^+$  exchange, we generated SV2A/2B- and SV2B/2C-double knockout (DKO) mice using the CRISPR/Cas9 system. We then tested if  $\text{Ca}^{2+}/\text{H}^+$  exchange activity was affected. Western blot analysis of LP2 fractions purified from SV2A/2B-DKO or SV2B/2C-DKO mice using isoform-specific antibodies confirmed efficient gene knockout by the CRISPR/Cas9 system (Fig. 4a). Moreover, western blot analysis using a pan-SV2 antibody that equally recognizes all SV2 isoforms revealed that SV2A and SV2B represented the major SV2 isoforms in brain, and expression of SV2C was minor (Fig. 4a). As a control, we confirmed that expression of synaptophysin, an abundant SV protein<sup>34</sup>, was unaltered in SVs derived from SV2-deficient mice. As shown in Fig. 4b,  $\text{Ca}^{2+}/\text{H}^+$  exchange activity was normal in SVs from SV2A/2B-DKO mice, and the extent of alkalization induced by 50  $\mu\text{M}$   $\text{CaCl}_2$  was comparable to that observed in SVs from wild-type mice of the same age (Fig. 4b).

Levetiracetam (LEV, also known as Keppra® or E Keppra®) is an established second-generation antiepileptic drug, whose molecular target is SV2A<sup>35</sup>. LEV selectively binds to the cytoplasmic portion of SV2A<sup>35,36</sup> and potentially inhibits SV2A function<sup>36</sup>. The inability of LEV to inhibit  $\text{Ca}^{2+}/\text{H}^+$  exchange (Fig. 4c) in SVs from wild-type mice provided further support that SV2A was not responsible for the activity, although SV2B, another isoform of SV2s, was present in the SV preparation. To completely rule out the contribution of SV2A to  $\text{Ca}^{2+}/\text{H}^+$  exchange activity, we examined the effect of LEV on transport activity in SV2B/2C-DKO samples (note that only SV2A is present in SV2B/2C-DKO mice). Again, LEV did not reduce  $\text{Ca}^{2+}$ -induced alkalization (Fig. 4d). Taken together, although SV2s have been proposed to function as  $\text{Ca}^{2+}$  transporters in SVs, SV2s do not contribute to high affinity  $\text{Ca}^{2+}/\text{H}^+$  exchange activity at neutral pH.

**The plasma membrane  $\text{Ca}^{2+}$  ATPases (PMCAs) mediate  $\text{Ca}^{2+}/\text{H}^+$  exchange in SVs.** Next, we examined the effect of blockers that selectively inhibit the P-type  $\text{Ca}^{2+}$  ATPases, including PMCAs and SERCA. Among the available inhibitors, 500  $\mu\text{M}$  vanadate, a PMCA blocker, potently inhibited  $\text{Ca}^{2+}$ -induced alkalization of SVs (Fig. 5a). On the other hand, 15  $\mu\text{M}$  cyclopiazonic acid (CPA), a SERCA inhibitor<sup>37</sup>, did not affect alkalization by  $\text{Ca}^{2+}$  (Fig. 5b), indicating that the high affinity  $\text{Ca}^{2+}/\text{H}^+$  exchange activity observed with this assay was attributed to PMCAs. Notably, whereas  $\text{Ba}^{2+}$ - and  $\text{Sr}^{2+}$ -induced alkalization of pre-acidified SVs by glutamate was largely abolished in the presence of vanadate, alkalization induced by  $\text{Zn}^{2+}$  or  $\text{Cd}^{2+}$  was not completely blocked by vanadate (Supplementary Fig. 4). These observations implied that, while  $\text{Ba}^{2+}$  and  $\text{Sr}^{2+}$  are recognized by PMCAs, there are other divalent cation/ $\text{H}^+$  exchangers that transfer  $\text{Zn}^{2+}$  or  $\text{Cd}^{2+}$ . Of note, ZnT-3, a vesicular  $\text{Zn}^{2+}$  transporter, is present on a subpopulation of SVs that contain glutamate<sup>38–40</sup>, and therefore could contribute to vanadate-insensitive  $\text{Zn}^{2+}/\text{H}^+$  exchange activity observed here, although the precise mechanism of  $\text{Zn}^{2+}$  transport into SVs, e.g. proton coupling during transport cycles, remains to be determined.

It was previously reported that in sheep SVs, vanadate-sensitive  $\text{Ca}^{2+}$  transport activity was largely absent in the presence of  $>200 \mu\text{M}$   $\text{Ca}^{2+}$ <sup>22</sup>. However,  $\text{Ca}^{2+}$ -induced alkalization at neutral pH was evident by 500  $\mu\text{M}$   $\text{Ca}^{2+}$  under our assay conditions (Fig. 5c, black trace). More importantly, 500  $\mu\text{M}$  vanadate effectively impeded the alkalization (Fig. 5c, red trace), indicating that even in the presence of higher concentrations of  $\text{Ca}^{2+}$ ,  $\text{Ca}^{2+}$ -induced alkalization was mediated by PMCAs, irrespective of the  $\text{Ca}^{2+}$  concentrations within this range.

**The PMCAs, but not SV2s, are responsible for the majority of  $\text{Ca}^{2+}$  transport into SVs at neutral pH.** To verify if  $\text{Ca}^{2+}$ -induced alkalization observed in our assay conditions was correlated with  $\text{Ca}^{2+}$  transport by PMCAs, we next examined radioactive  $^{45}\text{Ca}^{2+}$  uptake in the presence of various inhibitors. For this purpose, LP2 fraction was further purified by applying it to sucrose gradient centrifugation to minimize the contamination of other organelles and membranes. Consistent with the previous report<sup>22</sup>,  $^{45}\text{Ca}^{2+}$  uptake was suppressed by PMCA inhibitors (10  $\mu\text{M}$  eosin and 500  $\mu\text{M}$  vanadate) to background levels measured in the absence of ATP (Fig. 6a). In contrast, the V-ATPase inhibitor, bafilomycin (500 nM), did not affect  $^{45}\text{Ca}^{2+}$  uptake (Fig. 6b). Collectively, these results indicate that PMCAs are responsible for the majority of  $\text{Ca}^{2+}$  transport into SVs. In agreement with the results from acidification assays using SV2-KO vesicles,  $^{45}\text{Ca}^{2+}$  uptake into SVs derived from SV2A/SV2B-DKO mice (which lack the majority of SV2 proteins) was not significantly different from that derived from wild-type mice (Fig. 6c). Likewise, addition of 30  $\mu\text{M}$  LEV did not reduce  $\text{Ca}^{2+}$  transport into SVs derived from SV2B/2C-DKO mice (Fig. 6d), excluding the possibility that SV2s play a role in  $\text{Ca}^{2+}$  transport into SVs.

**PMCA1-pHluorin localizes in acidic compartments at presynaptic terminals.** The biochemical data described have demonstrated that PMCAs were responsible for the majority of  $\text{Ca}^{2+}$  transport into SV-rich membrane fractions, but it remains unclear whether they localized in functionally competent SVs in living neurons. In fact, isolated SVs from rodent brains contain various endosomal proteins such as endosomal SNAREs and rab proteins that may preferentially localize non-recycling vesicles at presynaptic terminals<sup>34</sup>. To clarify whether

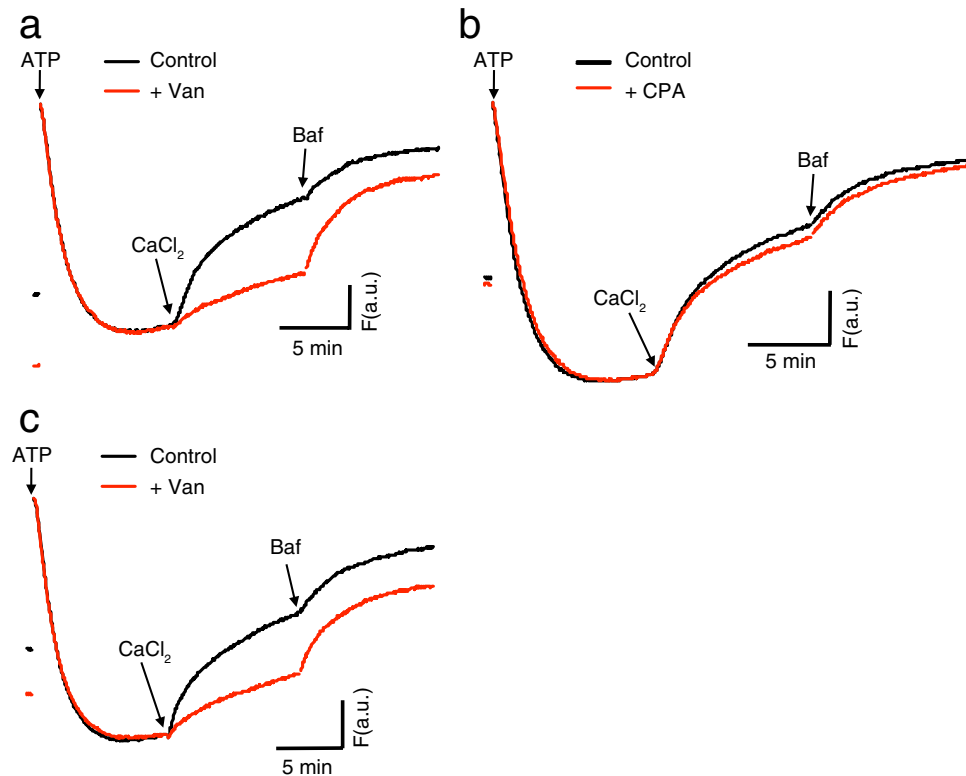


**Figure 5.** PMCA<sub>1</sub>s predominantly contribute to Ca<sup>2+</sup>/H<sup>+</sup> exchange. **(a)** Effect of vanadate (Van, 500 μM) on Ca<sup>2+</sup>-induced alkalization. Vesicles were pre-acidified in the presence of 5 mM glutamate and 3 mM KCl in the absence (black) and presence (red) of 500 μM Van, and 50 μM CaCl<sub>2</sub> was added to induce alkalization. **(b)** Effect of CPA (CPA, 15 μM) on Ca<sup>2+</sup>-induced alkalization. Vesicles were pre-acidified in the presence of 5 mM glutamate and 3 mM KCl in the absence (black) and presence (red) of 15 μM CPA, and 50 μM CaCl<sub>2</sub> was added to induce alkalization. **(c)** Effect of vanadate (Van, 500 μM) on Ca<sup>2+</sup>-induced alkalization by 500 μM CaCl<sub>2</sub>. Measurements were performed as in **(a)** except that a high concentration of CaCl<sub>2</sub> (500 μM) was added. All traces are the representative data from at least two to three measurements in each condition. Since vanadate slightly reduced AO quenching signals in the presence of 5 mM glutamate and 3 mM KCl, fluorescence traces were normalized by amplitudes of acidification, and the starting points of alkalization by CaCl<sub>2</sub> were adjusted for comparison.

PMCA<sub>1</sub>s localized at recycling or non-recycling vesicles in living neurons, we constructed a fluorescent reporter in which a pH-sensitive green fluorescent protein (super-ecliptic pHluorin; SEP<sup>30</sup>) was conjugated to the first luminal loop of PMCA<sub>1</sub> (Fig. 7a). A SEP fused to the second luminal loop of synaptophysin (SypHy) and a SEP fused to the C-terminal end of Syntaxin1a (Syntaxin1a-SEP) were used as controls for SV residents and plasma membrane residents, respectively (Fig. 7a). Due to the pH sensitivity of the reporter, fluorescence is quenched in acidic compartments whereas it rises when the reporter is exposed to the neutral pH solution in the extracellular space<sup>30</sup>. When PMCA<sub>1</sub>-SEP was transiently expressed in cultured hippocampal neurons derived from embryonic mouse brains, immunostaining of the fixed cells with an anti-GFP antibody revealed ubiquitous expression of PMCA<sub>1</sub>-SEP in cell bodies and dendrites (Fig. 7b, left), as well as in presynaptic bouton-like structures (Fig. 7b, right). Co-immunostaining with an antibody against synaptophysin further confirmed the presynaptic localization of PMCA<sub>1</sub>-SEP (Fig. 7b, right panels). Estimation of inner/surface distribution of PMCA<sub>1</sub>-SEP by sequential applications of an acidic solution (pH 5.5) and a 50 mM NH<sub>4</sub>Cl solution<sup>41</sup> indicated that ~75% of PMCA<sub>1</sub>-SEP was localized in the acidic compartments whose average pH was  $6.47 \pm 0.03$  (Fig. 7d,e, Supplementary Fig. 5). Control experiments with SypHy revealed that ~80% of SypHy was localized in the acidic compartments whose average luminal pH was  $\sim 5.91 \pm 0.02$ . In contrast, control experiments with Syntaxin1a-SEP revealed that it was localized almost exclusively on the plasma membrane ( $99.5 \pm 2.2\%$ ) (Fig. 7c-e, Supplementary Fig. 5). The higher luminal pH of PMCA<sub>1</sub>-pHluorin-positive vesicles indicates that a portion of PMCA<sub>1</sub>-pHluorin may localize in endosomal compartments. Alternatively, exogenous expression of PMCA<sub>1</sub>-pHluorin may exert additional Ca<sup>2+</sup>/H<sup>+</sup> antiport, which would facilitate alkalization of the vesicular lumen. Collectively, although PMCA<sub>1</sub>-SEP expression was not restricted to the presynaptic terminals in cultured hippocampal neurons, a fraction of PMCA<sub>1</sub>-SEP did seem to be localized in the acidic compartments whose luminal pH was similar to that of typical SVs.

**PMCA<sub>1</sub>-SEP recycles at presynaptic terminals.** To examine whether PMCA<sub>1</sub>-SEP-positive vesicles would recycle at presynaptic terminals in an activity-dependent manner, cultured hippocampal neurons

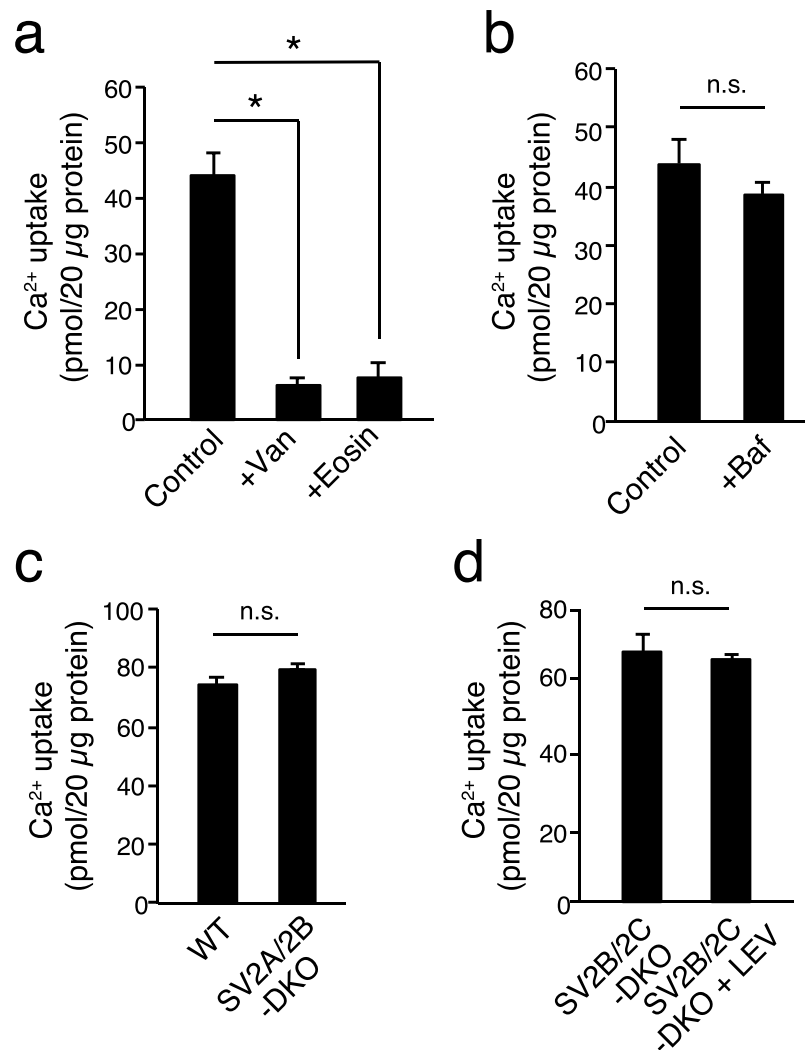


**Figure 6.** PMCAs predominantly contribute to  $\text{Ca}^{2+}$  uptake into SVs independent of  $\text{H}^+$  electrochemical gradient generated by V-ATPase. **(a)**  $\text{Ca}^{2+}$  transport was measured using  $^{45}\text{Ca}^{2+}$  as a tracer. The assay was performed in the absence of inhibitors (Control) or in the presence of vanadate (Van, 500  $\mu\text{M}$ ) or eosin (10  $\mu\text{M}$ ). Both PMCA blockers effectively inhibited  $\text{Ca}^{2+}$  transport into the SV fraction. Error bars indicate s.e.m. of three independent measurements. \* $p < 0.0025$ , unpaired equal variance Student's *t*-test. **(b)**  $\text{Ca}^{2+}$  transport was measured as in (a) in the absence (Control) and presence of the V-ATPase inhibitor, bafilomycin A (500 nM) (Baf). Error bars indicate s.e.m. of three measurements. n.s. indicates not significant ( $p > 0.1$ , unpaired equal variance Student's *t*-test). **(c)**  $\text{Ca}^{2+}$  transport into LP2 from wild-type mice (WT) and that from SV2A/2B-DKO mice were measured. Error bars indicate s.e.m. of three measurements. n.s. indicates not significant ( $p > 0.1$ , unpaired equal variance Student's *t*-test). **(d)**  $\text{Ca}^{2+}$  transport into LP2 from SV2B/2C-DKO mice in the absence or presence of 30  $\mu\text{M}$  levetiracetam (LEV) were compared. Error bars indicate s.e.m. of three measurements. n.s. indicates not significant ( $p > 0.1$ , unpaired equal variance Student's *t*-test).

expressing PMCA1-SEP were exposed to repetitive electrical stimulation (Fig. 8). At the end of recordings, 50 mM  $\text{NH}_4\text{Cl}$  solution was applied to estimate the total fluorescence of the SEP molecules (Fig. 8a). Notably, PMCA1-SEP fluorescence increased upon repetitive stimulation at 20 Hz for 10 sec in a manner similar to that of SypHy (Fig. 8a), although the fraction of PMCA1-SEP molecules engaged in exocytosis during stimulation was significantly less than that of SypHy (Fig. 8b). In accordance with the slightly higher vesicular pH of the PMCA1-carrying vesicles (Fig. 7e), this indicated that compared to synaptophysin, more PMCA1 was localized in non-recycling acidic compartments such as endosomes. The kinetics of the rise phase (mainly reflecting exocytosis) and decay phase (reflecting endocytosis and subsequent re-acidification of endocytosed vesicles) were identical to those of SypHy (Fig. 8c-e). Furthermore, when neurons were treated with 10 nM tetanus toxin (TeNT), which cleaves the major vesicular SNARE (v-SNARE) synaptobrevin/VAMP2<sup>42</sup>, PMCA1-SEP responses were completely abolished (Fig. 8f, Supplementary Fig. 6). This effect was also observed for SypHy (Fig. 8f, Supplementary Fig. 6), indicating that PMCA1 was present on synaptobrevin/VAMP2-positive vesicles and followed the same fate as that of synaptobrevin/VAMP2 during activity-dependent SV recycling.



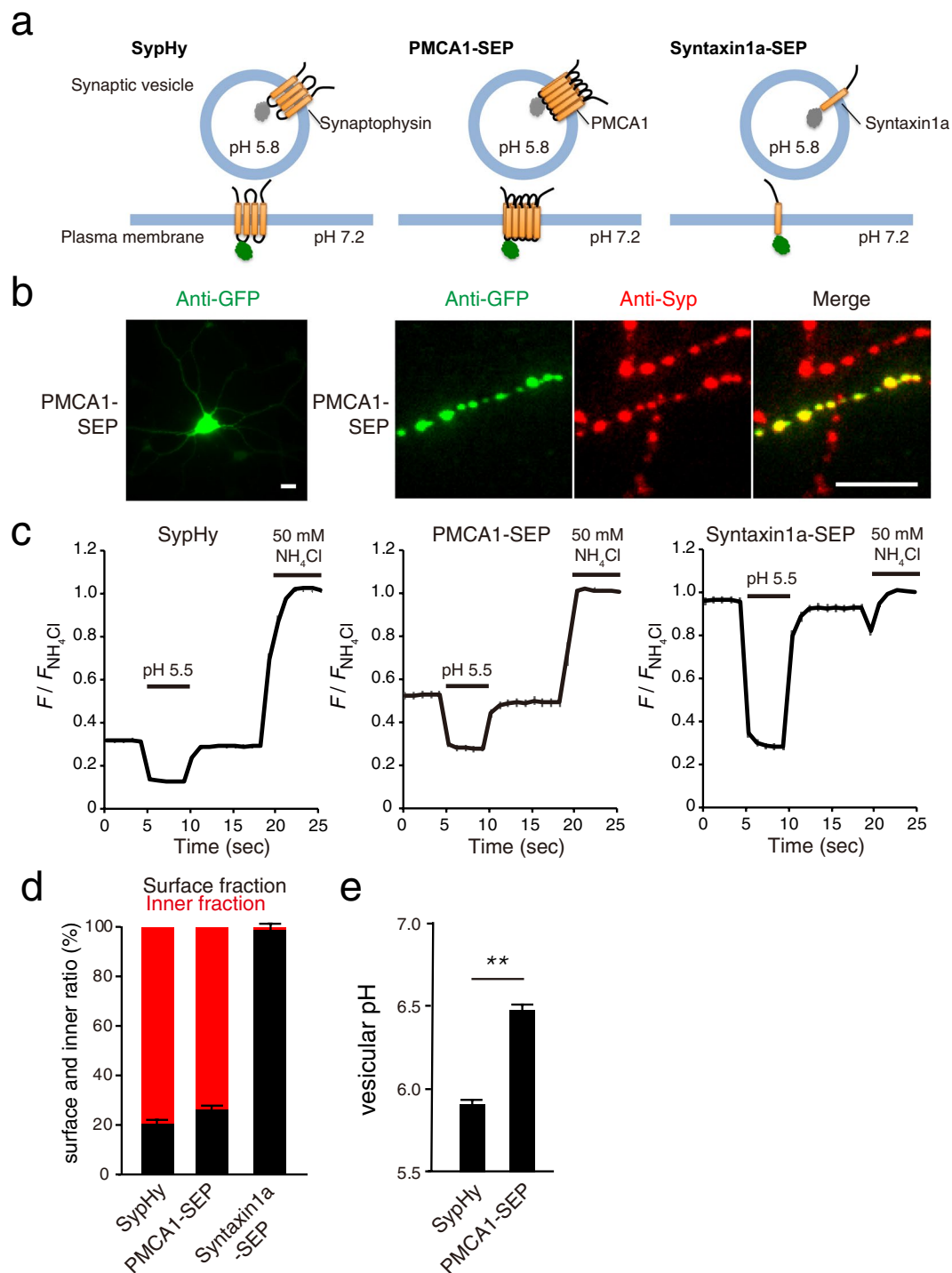


**Figure 7.** Localization of PMCA1-pHluorin in acidic compartments at presynaptic terminals of cultured hippocampal neurons. **(a)** Schematic diagrams of the pHluorin probes. The super-ecliptic pHluorin (SEP) was fused either to the second luminal loop of synaptophysin (SypHy), to the first luminal loop of PMCA1 (PMCA1-SEP), or to the C-terminal end of syntaxin1a (Syntaxin1a-SEP). When these proteins reside on synaptic vesicle membranes, the SEP fluorescence is quenched due to the acidic pH (~5.8), whereas they become fluorescent when they are present at the plasma membrane and are thereby exposed to the extracellular neutral pH (~7.2). **(b)** Fluorescence images of cultured hippocampal neurons expressing PMCA1-SEP. PMCA1-SEP was visualized by immunostaining with rabbit polyclonal anti-GFP antibody (green). A synaptic vesicle marker, synaptophysin, was visualized by immunostaining with mouse monoclonal anti-synaptophysin antibody (red). The right panels show merged pictures of the two immunostainings. Scale bars indicate 10  $\mu\text{m}$  (cell body in the left panel) and 5  $\mu\text{m}$  (right panels). **(c)** Average fluorescence of SypHy (left,  $n = 100$  boutons from 10 images), PMCA1-SEP (middle,  $n = 99$  from 10 images), and Syntaxin1a-SEP (right,  $n = 100$  from 10 images) in response to sequential application of a pH 5.5 solution and 50 mM  $\text{NH}_4\text{Cl}$ . After baseline subtraction, fluorescence of bouton-like structures were normalized to those during 50 mM  $\text{NH}_4\text{Cl}$  application. **(d)** Distribution of SypHy,

PMCA1-SEP, and Syntaxin1a-SEP between cell surface (black bars) and acidic intracellular compartment (red bars) deduced from the traces in (c). Error bars indicate s.e.m. for the cell surface fraction. (e) Luminal pHs of vesicles carrying SypHy or PMCA1-SEP deduced from the traces in (c). Error bars indicate s.e.m. \*\* $p < 0.00025$ , unpaired unequal variance Student's  $t$ -test.

## Discussion

In this study, we characterized the biochemical properties of  $\text{Ca}^{2+}$  transport into SVs isolated from rodent brains. We found that PMCA, the plasma membrane  $\text{Ca}^{2+}$  ATPases, confer the majority of  $\text{Ca}^{2+}$  transport into SVs. Previous studies have indicated that there are two  $\text{Ca}^{2+}$  transport systems in isolated SVs; one is mediated by PMCA at neutral pH, and the other is mediated by an independent  $\text{Ca}^{2+}/\text{H}^{+}$  exchanger at alkaline pH. Our results strongly support a united model indicating that PMCA is solely responsible for both activities in the majority of the SV population at neutral pH. Novel findings extending beyond those of previous studies<sup>21–23,29</sup> are as follows. First, even at neutral pH of the extra-vesicular space,  $\text{Ca}^{2+}$  alkalized pre-acidified SV lumen. This phenomenon became evident when BAPTA was used to control free  $\text{Ca}^{2+}$  concentrations, although we currently do not understand why the use of EGTA attenuated alkalization signals in the acidification assays. Since the SV alkalization by  $\text{Ca}^{2+}$  was restored by vanadate which concomitantly impeded  $^{45}\text{Ca}$  uptake into SVs, we conclude that PMCA is responsible for  $\text{Ca}^{2+}/\text{H}^{+}$  exchange activity. This is consistent with more recent findings that counter transport of  $\text{H}^{+}$  is associated with  $\text{Ca}^{2+}$  transport by PMCA<sup>43</sup>. Second, the  $\text{Ca}^{2+}/\text{H}^{+}$  exchange at neutral pH exhibited high affinity for  $\text{Ca}^{2+}$  ( $K_m \sim 400 \text{ nM}$ ) that was similar to the reported values for PMCA<sup>44</sup>, whereas previously reported  $\text{Ca}^{2+}/\text{H}^{+}$  exchange activity at alkaline pH was characterized as a low affinity  $\text{Ca}^{2+}/\text{H}^{+}$  exchanger ( $K_{0.5} \sim 217 \mu\text{M}$ )<sup>22</sup>. Third, although PMCA has been characterized as residing in the plasma membrane, our imaging analysis revealed that PMCA was potentially capable of recycling in an activity-dependent manner at presynaptic terminals. This observation was further substantiated by the fact that recycling of PMCA1-SEP depended exclusively on the presence of synaptobrevin/VAMP2 on the same vesicles, which is essential for stimulus-dependent exocytosis of SVs<sup>45</sup>.

Our results are highly consistent with biochemical evidence that, in addition to V-type  $\text{H}^{+}$  ATPases, vanadate-sensitive P-type ATPases constitute the major ATPases in cholinergic SVs from Torpedo electric organs<sup>46</sup> as well as clathrin-coated vesicles from bovine brains<sup>47</sup>. Although PMCA, which are P-type ATPases, have been characterized as plasma membrane residents, our results demonstrate that PMCA constitute the major ATPase on recycling SVs as well. This is also consistent with proteomic analyses that identified PMCA within SV fractions<sup>34,48</sup>. Thus, besides the main role of PMCA in excluding  $\text{Ca}^{2+}$  from the presynaptic cytosol to the extracellular space at the plasma membrane, vesicular PMCA may also contribute to  $\text{Ca}^{2+}$  clearance from the presynaptic cytosol. Furthermore, since  $\text{Ca}^{2+}$  transport into SVs is coupled to  $\text{H}^{+}$  efflux, vesicular PMCA may be involved in the regulation of  $\Delta\mu\text{H}^{+}$  of SVs, which drives neurotransmitter uptake into SVs. Indeed, external (cytosolic)  $\text{Ca}^{2+}$  strongly inhibited dopamine uptake into isolated SV fraction<sup>49</sup>, which is reasonable given that  $\Delta\text{pH}$ , the driving force for dopamine uptake, is attenuated by  $\text{Ca}^{2+}/\text{H}^{+}$  exchange. In contrast, glutamate uptake, which is predominantly driven by  $\Delta\Psi$ , was only marginally facilitated under the condition where  $\Delta\Psi$  predominated in the presence of  $17 \text{ mM Cl}^{-}$ <sup>49</sup>. This subtle effect by  $\text{Ca}^{2+}$  on glutamate transport indicates that PMCA on SVs are electro-neutral pumps ( $\text{Ca}^{2+}:\text{H}^{+} = 1:2$ ), which is consistent with observations in snail neurons<sup>43</sup>. Alternatively, the fact that glutamate transport in the presence of  $\text{Ca}^{2+}$  retained a typical biphasic  $\text{Cl}^{-}$  dependency<sup>49</sup> (note that increasing  $\text{Cl}^{-}$  concentrations build up greater  $\Delta\text{pH}$ ) may indicate an important contribution of protons (or vesicular pH) on VGLUT function<sup>2–4</sup>. Further investigations will be needed to clarify how  $\text{Ca}^{2+}/\text{H}^{+}$  exchangers in conjunction with vesicular  $\text{Cl}^{-}$  carriers, either VGLUTs or the  $\text{ClC}$ -type  $\text{Cl}^{-}$  transporters, affect glutamate transport into SVs.

The plasma membrane PMCA is responsible for transient acidification of the cytoplasm during sustained stimulation at mouse motor nerve terminals, which may regulate endocytosis<sup>31</sup>. Our imaging analysis indicated that a substantial portion of vesicular PMCA is inserted into the plasma membrane by exocytosis and retained there until endocytosis is completed, indicating that the total PMCA expression on the plasma membrane increases, especially during high activity. Although the contribution of the vesicular PMCA that are inserted into the plasma membrane to acidification of the cytoplasm seems to be negligible<sup>31</sup>, it remains to be determined to what extent  $\text{Ca}^{2+}$  extrusion from the cytoplasm is accelerated by the vesicular PMCA that translocate into the plasma membrane during high neural activity.

In mammals, four different genes encode the four isoforms of PMCA<sup>50</sup>. PMCA1 and PMCA4 are expressed ubiquitously, whereas PMCA2 and PMCA3 are expressed predominantly in the central nervous system. Furthermore, each isoform has multiple splice variants, comprising more than 30 spliced isoforms, although little is known about the functional significance of multiple splice variants<sup>50</sup>. In this study, we show that one of the PMCA, the full length PMCA1 (1,249 a.a.) fused to pHluorin at its luminal region, is sorted preferentially to recycling SVs rather than to the plasma membrane at presynaptic terminals, and its distribution and recycling behaviors are very similar to those of the SV marker, synaptophysin (Figs 7 and 8). It remains unknown whether other PMCA isoforms or respective splice variants show similar properties to those of the full length PMCA1-pHluorin at presynaptic terminals, which may necessitate more complex regulation of  $\text{Ca}^{2+}$  and  $\text{H}^{+}$  dynamics at presynaptic terminals. Additionally, it should be kept in mind that we still lack concrete evidence for the existence of PMCA proteins on SVs, as the evidence we provide in this study relies on the usage of pharmacological blockade of  $\text{Ca}^{2+}$  transport by PMCA blockers and also on the exogenous expression of PMCA1 fused to fluorescent proteins. Although the SV proteome supports the existence of PMCA in the SV fraction isolated from native brains<sup>32</sup>, previous fractionation experiments, combined with western blot analysis using isoform-specific PMCA antibodies, have provided controversial results concerning the localization of PMCA isoforms in synaptic

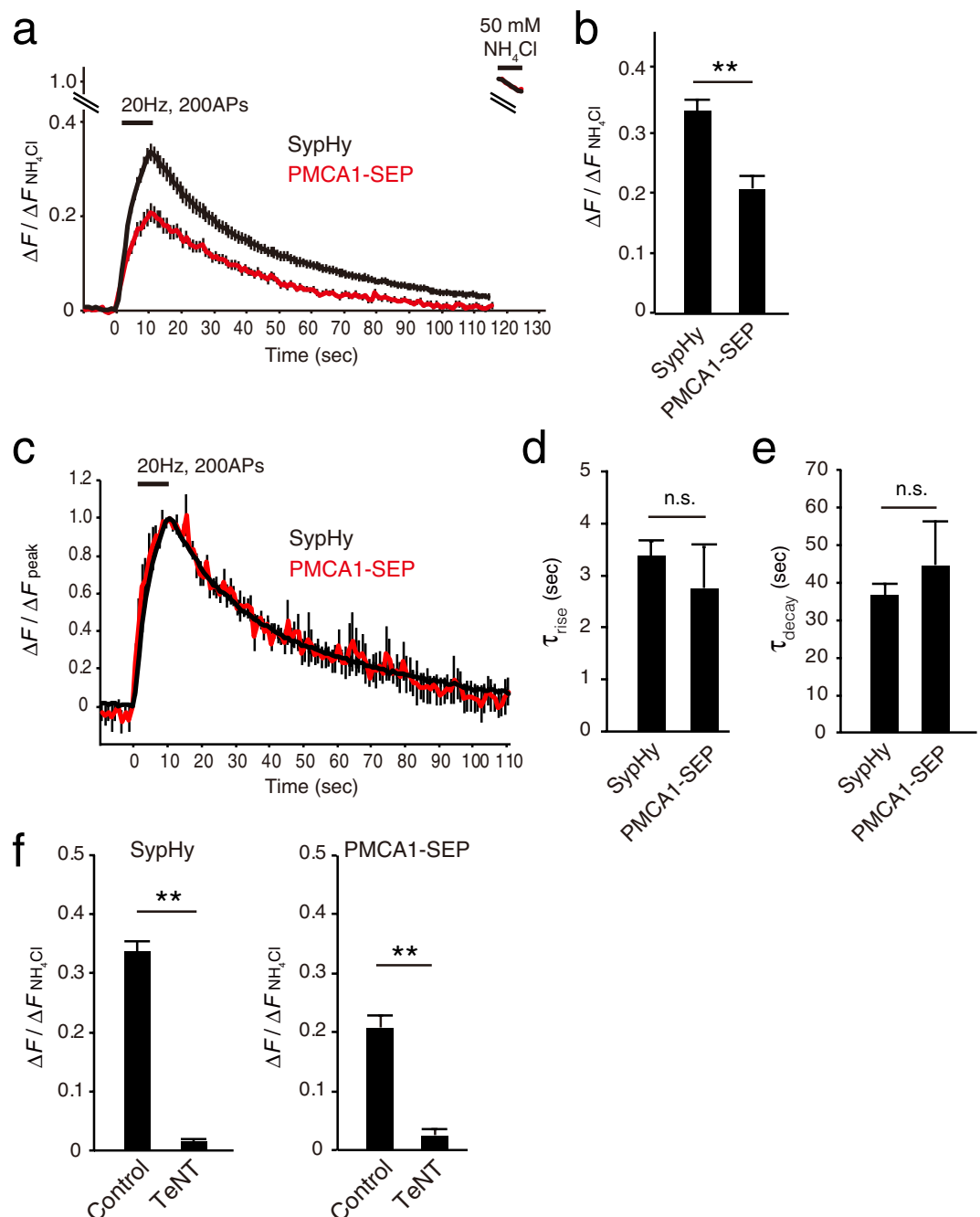


**Figure 8.** Activity-dependent recycling of PMCA1-pHluorin at presynaptic terminals. **(a)** SypHy (black;  $n = 100$  boutons from 10 images) and PMCA1-SEP (red;  $n = 53$  from 6 images) fluorescence in response to 200 action potentials (APs) at 20 Hz. Fluorescence signals were normalized to those obtained during  $\text{NH}_4\text{Cl}$  application at the end of recordings. **(b)** Peak fluorescence of SypHy and PMCA1-SEP at the end of field stimulation. Error bars indicate s.e.m.  $**p < 0.00025$ , unpaired unequal variance Student's  $t$ -test. **(c)** Superimposed traces of SypHy (black) and PMCA1-SEP (red). The traces in **(a)** were normalized to the peak fluorescence at the end of repetitive stimulation. **(d)** Time constants of the rise time during stimulation. Exocytic rise phases were fitted with single exponentials and time constants ( $\tau_{\text{rise}}$ ) were deduced by using the Solver function in Excel software. An average from one image was taken as  $n = 1$ . Error bars indicate s.e.m. n.s. indicates  $p > 0.1$ , unpaired equal variance Student's  $t$ -test. **(e)** Time constants of the decay phases after the cessation of stimuli. Decay traces were fitted with single exponentials and endocytic time constants ( $\tau_{\text{decay}}$ ) were deduced using the Solver function in Excel software. An average from one image was taken as  $n = 1$ . Error bars indicate s.e.m. n.s. indicates  $p > 0.1$ , unpaired equal variance Student's  $t$ -test. **(f)** SypHy (left;  $n = 88$  boutons from 9 images) and PMCA1-SEP (right;  $n = 72$  boutons from 8 images) fluorescence in response to 200 APs at 20 Hz without (Control) or with 16 hours tetanus toxin treatment (TeNT, 10 nM). Bars indicate peak fluorescence of SypHy and PMCA1 at the end of stimulation with or without tetanus toxin pretreatment. Error bars indicate s.e.m.  $**p < 0.00025$ , unpaired unequal variance Student's  $t$ -test.

vesicles<sup>49,50</sup>, probably due to their predominant expression at the plasma membrane of the cell body. Thus, direct demonstration of PMCA isoforms on synaptic vesicles, e.g. via immuno-gold labeling of isolated SV fractions or immuno-gold labeling of brain sections, will be essential to confirm their vesicular localization in the future.

SV2s are postulated to function as a  $\text{Ca}^{2+}$  transporter, since synaptic phenotypes observed in SV2-deficient mice could be well explained if SV2s function as  $\text{Ca}^{2+}$  transporters<sup>26,27</sup>. However, our results from direct tests of  $\text{Ca}^{2+}$  transport into SV2-deficient vesicles rule out this hypothesis (Figs 4 and 6). Therefore, the  $\text{Ca}^{2+}$ -related phenotypes observed previously in SV2-deficient mice may be indirect consequences of unknown functions of SV2. Of note, it has recently been shown that SV2A mediates galactose/ $\text{H}^+$  symport when heterologously expressed in yeast cells<sup>51</sup>. Although the functional significance of galactose in the nervous system, particularly its role in SVs, has been enigmatic, changes in either metabolism of carbohydrates or composition of glycans attached to proteins or lipids may indirectly regulate  $\text{Ca}^{2+}$  homeostasis at presynaptic terminals, which would lead to the observed  $\text{Ca}^{2+}$ -related phenotypes in SV2-deficient synapses. Uncovering the link between SV2s' function and presynaptic [ $\text{Ca}^{2+}$ ] regulation will help to elucidate the role of SV2s in epileptogenesis caused by SV2A gene knockout<sup>26,52</sup>.

In summary, our present results collectively suggest that  $\text{Ca}^{2+}$  transport across SV membranes is predominantly, if not exclusively, mediated by PMCA. Due to their property as  $\text{Ca}^{2+}/\text{H}^+$  exchangers, PMCA may contribute to the regulation of  $\Delta\mu\text{H}^+$  and the dynamic control of cytosolic  $\text{Ca}^{2+}$  and  $\text{H}^+$  at presynaptic terminals. Since various single nucleotide polymorphisms (SNPs) have been identified in PMCA genes that are associated with neuronal disorders such as autism and deafness<sup>53</sup>, it will be crucial to establish how these SNPs affect the function and distribution of PMCA in neurons to elucidate the mechanisms underlying these diseases.

## Materials and Methods

**Synaptic vesicle isolation.** Crude synaptic vesicle fraction (LP2) was isolated from mouse whole brains with slight modifications<sup>54</sup>. Briefly, whole brains from C57BL/6 mice were homogenized in homogenization buffer (320 mM sucrose, 4 mM  $\text{MgSO}_4$ , 4 mM HEPES- $\text{NaOH}$ , pH 7.3). The homogenate was centrifuged for 10 min at  $1,000 \times g$ , the resulting supernatant (S1) was centrifuged for 15 min at  $12,000 \times g$ . The resulting pellet (P2) was washed with homogenization buffer and re-centrifuged for 15 min at  $13,000 \times g$  to obtain crude synaptosomes (P2'). To release SVs from the synaptosomes, P2' fraction was subjected to an osmotic shock by the addition of 9 volume of ice-cold water and the subsequent homogenization. The resulting suspension was centrifuged for 20 min at  $33,000 \times g$ . After centrifugation, the supernatant (LS1; lysate supernatant) was centrifuged for 2 hours at  $260,000 \times g$ . The final membrane pellet (LP2) was resuspended in standard acidification buffer (300 mM sucrose, 4 mM  $\text{MgSO}_4$ , 10 or 20 mM MOPS-KOH, pH 7.2), and stored at  $-80^\circ\text{C}$  until use. Essentially, all fluorometric assays, unless indicated otherwise, were performed with this fraction. For determination of apparent affinity of  $\text{Ca}^{2+}/\text{H}^+$  exchange activity and radioactive<sup>45</sup>  $\text{Ca}^{2+}$  uptake, LP2 obtained from Wistar rat brains was further purified by sucrose gradient centrifugation (50–800 mM continuous gradient). After centrifugation at  $65,000 \times g_{max}$  for 4 hours, turbid materials visible in the middle of the gradient (in the range of 200 to 400 mM sucrose) were pooled and sedimented by centrifugation at  $260,000 \times g_{max}$  for 90 min. The resulting pellet (SV) was resuspended in acidification buffer and stored at  $-80^\circ\text{C}$  until use.

**Calculation of free  $\text{Ca}^{2+}$  concentrations.** Free calcium concentration was calculated by solving simultaneous equations in four unknowns: concentration of  $\text{Ca}^{2+}$  binding with BAPTA ([CaBAPTA]), concentration of  $\text{Mg}^{2+}$  binding with BAPTA ([MgBAPTA]), concentration of  $\text{Mg}^{2+}$  binding with ATP ([MgATP]) and that of  $\text{Ca}^{2+}$  binding with ATP ([CaATP]) as follows.

$$K'_{\text{CaBAPTA}} = \frac{[\text{CaBAPTA}]}{([\text{Ca}^{2+}]_T - [\text{CaBAPTA}] - [\text{CaATP}])([\text{BAPTA}]_T - [\text{CaBAPTA}] - [\text{MgBAPTA}])}$$

$$K'_{\text{MgBAPTA}} = \frac{[\text{MgBAPTA}]}{([\text{Mg}^{2+}]_T - [\text{MgBAPTA}] - [\text{MgATP}])([\text{BAPTA}]_T - [\text{CaBAPTA}] - [\text{MgBAPTA}])}$$

$$K'_{\text{CaATP}} = \frac{[\text{CaATP}]}{([\text{Ca}^{2+}]_T - [\text{CaBAPTA}] - [\text{CaATP}])([\text{ATP}]_T - [\text{CaATP}] - [\text{MgATP}])}$$

$$K'_{\text{MgATP}} = \frac{[\text{MgATP}]}{([\text{Mg}^{2+}]_T - [\text{MgBAPTA}] - [\text{MgATP}])([\text{ATP}]_T - [\text{CaATP}] - [\text{MgATP}])}$$

$[\text{Ca}^{2+}]_T$ ,  $[\text{Mg}^{2+}]_T$ ,  $[\text{BAPTA}]_T$  and  $[\text{ATP}]_T$  are the total concentrations of each substance.  $[\text{Ca}^{2+}]_T$  is calculated from an equation  $[\text{Ca}^{2+}]_T = [\text{Ca}^{2+}]_{\text{add}} + [\text{Ca}^{2+}]_{\text{ctm}}$ , where  $[\text{Ca}^{2+}]_{\text{add}}$  and  $[\text{Ca}^{2+}]_{\text{ctm}}$  are concentration of added  $\text{CaCl}_2$  and of contaminated  $\text{Ca}^{2+}$  determined routinely by fura-2 assay, respectively.  $K'_{\text{CaBAPTA}}$ ,  $K'_{\text{MgBAPTA}}$ ,  $K'_{\text{CaATP}}$  and  $K'_{\text{MgATP}}$  are the overall apparent association constants. Microsoft Excel Solver was used to solve the equations.

To set up the equations above, the overall apparent association constants,  $K'$ 's ( $K'_{\text{CaBAPTA}}$ ,  $K'_{\text{MgBAPTA}}$ ,  $K'_{\text{MgATP}}$  and  $K'_{\text{CaATP}}$ ) were converted from the absolute association constants,  $K_s$ , which were determined for standard conditions (see details in Marks and Maxfield<sup>55</sup>). Supplementary Table 1 lists the published association constants for BAPTA and ATP, as well as the  $\Delta H$  values for BAPTA and ATP.  $\Delta H$  values were necessary for the conversions from the absolute association constants to the overall apparent association constants.

**Acidification assay.** Acidification measurements were performed according to previous publications using acridine orange (AO, Molecular Probes) as a  $\Delta\text{pH}$  reporter<sup>3</sup>. Changes in AO fluorescence (excitation at 492 nm and emission at 530 nm with slit lengths with 2.5 nm, HMT 700 V) were monitored in a Hitachi F2500 fluorometer

(Hitachi, Japan) at 32 °C, unless otherwise stated<sup>3</sup>. Typically, 20 µg of LP2 or SV fraction was preincubated in 1 mL of assay buffer (300 mM sucrose, 4 mM MgSO<sub>4</sub>, 1.5 µM AO, 10 or 20 mM MOPS, pH 7.2) with varying composition of 5 mM K-glutamate, 3 mM or 100 mM KCl, 50 µM EGTA, and 50 µM BAPTA as indicated in the figures or figure legends. After a stable baseline was achieved (usually within 10 min), 2 mM ATP was added to start acidification. Various concentrations of CaCl<sub>2</sub> or 50 µM other divalent cations were added at 10 min where indicated. At the end of recordings, a V-ATPase inhibitor, bafilomycin A<sub>1</sub> (500 nM) was added to ensure that quenching of AO was due to proton translocation by the V-ATPase. For Figs 4 and 5, 15 µM cyclopiazonic acid, 500 µM vanadate, or 30 µM levetiracetam was pre-incubated for 5 min before measurements. Representative traces from multiple measurements are shown in the figures. For estimation of temperature co-efficient (Q<sub>10</sub>) for the Ca<sup>2+</sup>-dependent AO de-quenching, acidification assays were performed at two different temperatures. The Q<sub>10</sub> was calculated from an equation:

$$Q_{10} = \left( \frac{\tau_1}{\tau_2} \right)^{\left( \frac{10}{T_2 - T_1} \right)},$$

in which  $\tau_1$  and  $\tau_2$  are time constants of recovery phases of acridine orange fluorescence after the addition of Ca<sup>2+</sup> at temperature T<sub>1</sub> and T<sub>2</sub>.  $\tau_1$  and  $\tau_2$  were obtained by a first order exponential fitting using a Solver function in Excel software. T<sub>1</sub> and T<sub>2</sub> (T<sub>2</sub> > T<sub>1</sub>) are 32.3 and 37.3 °C, respectively.

**Fura-2 assay.** Ca<sup>2+</sup> concentrations in some experimental solution were measured using fura-2 (pentapotassium salt, impermeant, Invitrogen) as a Ca<sup>2+</sup> reporter. Changes in fura-2 fluorescence (excitation at 340 nm and emission at 510 nm, with slit lengths with 2.5 nm, HMT 400 V) were monitored in a Hitachi F2500 fluorometer (Hitachi, Japan) at 32 °C. 1 ml of an assay buffer (100 mM KCl, 10 mM MOPS-KOH, pH7.2) was preincubated for 10 min. The preincubation was followed by adding 300, 600, 900, 1200 and 1500 nM total exogenous CaCl<sub>2</sub> each with 30 sec intervals. At the end of recordings, 50 µM BAPTA was added to chelate exogenous and contaminated Ca<sup>2+</sup>.

**Animals.** C57BL/6Njcl mice were purchased from CLEA, Japan. ICR mice were purchased from SLC, Japan. All mice were given food and water *ad libitum*. Animals were kept in an SPF facility with a 12-hour light and 12-hour dark cycle. The ambient temperature was maintained around 21 °C with a relative humidity of 50%. ICR mice (12 to 20 weeks old) were used as recipients. A combination anesthetic (0.75 mg/kg of medetomidine, 4.0 mg/kg of midazolam, and 5.0 mg/kg of butorphanol) was used for surgery. The anesthetics were administered to recipient mice by intraperitoneal injection. All animal experiments were approved by the Institutional Animal Care and Use Committee of the RIKEN Kobe branch (approval number: QA2013-04-6) and the Institutional Animal Care and Use Committee of Doshisha University.

**One-cell embryo microinjection.** C57BL/6N females (4–6 weeks old) were superovulated and mated with C57BL/6N males. Fertilized eggs were collected from the ampulla of the oviduct of plugged C57BL/6N females by micro-dissection and kept in KSOM medium (Merck Millipore) in a 5% CO<sub>2</sub> incubator at 37 °C. *Cas9* mRNA (100 ng/µL) and six gRNAs (50 ng/µL each, 300 ng/µL total) were co-injected into the cytoplasm of fertilized eggs in M2 medium (Merck Millipore) at room temperature. Details of the cytoplasmic injection procedure have been described previously<sup>56</sup>. After microinjection, the injected embryos were cultured for 1 hr in KSOM medium (Merck Millipore) in a 5% CO<sub>2</sub> incubator at 37 °C, then 15–30 embryos were transferred to the oviducts of recipient ICR female mice.

**One-step generation of double gene knockouts of SV2A/2B and SV2B/2C.** Double gene knockout (DKO) mice of SV2A/2B and SV2B/2C were generated by the triple-target CRISPR method<sup>57</sup>. Briefly, *Cas9* mRNA and sgRNAs were synthesized according to the protocol reported previously<sup>57</sup>. All gRNAs were selected from pre-made design in Database (<http://crispr.riken.jp>). *Cas9* mRNA (100 ng/µL) and six gRNAs (50 ng/µL each, 300 ng/µL total) were injected into the cytoplasm of fertilized eggs of C57BL/6Njcl mice. For SV2A/2B DKO, six gRNA targets were used (Sv2a\_8 5'-AAGGCGAACGCATGGCAGAT-3', Sv2a\_9 5'-GCGTAAAGATCGGGAAGAAT-3', Sv2a\_25 5'-GGCAGCCTTCCTTATTGTGC-3', Sv2b\_28 5'-CTGGCAATCGAAGGGCAATC-3', Sv2b\_38 5'-GTGGACCCTCTTCTTCGTCT-3', Sv2b\_41 5'-AGGTATCGGGACAACACTATGA-3'). For SV2B/2C DKO, six gRNA targets were used (Sv2b\_28, Sv2b\_38, Sv2b\_41, Sv2c\_56 5'-ACTGGAATGGAATACGAGAA-3', Sv2c\_77 5'-AGACCTATGCATACCAAATT-3', Sv2c\_78 5'-CACAAACACCTCCACGCCAT-3').

**Ca<sup>2+</sup> transport assay.** The concentrations of SV or LP2 fractions were adjusted to 0.2 mg/mL in sucrose buffer. 100 µL aliquots were preincubated for 10 min at 32 °C. The reaction was started by addition of 10 µM (final concentration) <sup>45</sup>Ca<sup>2+</sup> dissolved in sucrose buffer containing ATP (2 mM), vanadate (500 µM), eosinY (10 µM), cyclopiazonic acid (15 µM) and levetiracetam (30 µM) when indicated. All incubations contained 0.125% (v/v) DMSO and 0.167% (v/v) ethanol in a final volume of 150 µL. After incubation for 10 min at 32 °C, the reaction was stopped by addition of 3 mL of ice-cold buffer, followed by filtration through nitrocellulose filters. The incubation tubes were washed out with 3 mL of ice-cold buffer, and the wash out buffer was poured through the filter. The filters were washed out twice with 2.5 mL of ice-cold buffer. Radioactivity retained on filters was measured by liquid scintillation counting using an ALOKA LSC-6100 liquid scintillation counter (ALOKA, Japan).

**Western blot analysis.** SDS-PAGE was used to separate 20 µg of LP2 fractions from wild-type or SV2-DKO mice. Proteins were transferred to a PVDF membrane. The resulting blots were probed with isoform specific

antibodies for SV2s (Synaptic Systems, Germany) or with a pan-SV2 monoclonal antibody (a kind gift from Reinhard Jahn, Göttingen, Germany). For detection, the appropriate secondary antibodies conjugated to horseradish peroxidase were used. After washing steps, the horseradish peroxidase was detected by enhanced chemiluminescence using a commercially available kit (Perkin Elmer, Inc., MA). As loading controls, anti-synaptophysin monoclonal antibody (C17.2, a gift from Reinhard Jahn' instead of 'Synaptic Systems, Germany') was used.

**Molecular biology.** To construct PMCA1-SEP, a full length mouse PMCA1 (accession no. NM\_001359506.1) was amplified by PCR from mouse adult brain cDNA generated using SuperScript RT-PCR system (Invitrogen) and subcloned into a *StuI* site of pCR-Blunt vector (Thermo Fisher Scientific). A DNA fragment encoding the N-terminal region of PMCA1 (a.a. 1–139) with linker sequence (STSGGSGGTGGS) and a fragment of super-ecliptic pHluorin (SEP) amplified from SypHy plasmid<sup>58,59</sup> (a kind gift from Leon Lagnado) were amplified by PCR and cloned into an *EcoRV* site of pcDNA3.1(+) using In-Fusion Cloning Kit (Clontech). A DNA fragment encoding the C-terminal region of PMCA1 (a.a. 140–1,220) was PCR-amplified and cloned into a *NotI* site of pcDNA3.1(+) which contained the N-terminal region of PMCA1 and SEP using In-Fusion Cloning Kit. To construct Syntaxin1a-SEP, a full length mouse Syntaxin-1a (accession no. NM\_016801.3) without the stop codon and a fragment of SEP were amplified by PCR and simultaneously cloned into a *NheI/EcoRV* site of pcDNA3.1(+). A DNA fragment encoding SypHy<sup>59</sup> was amplified by PCR and subcloned into a *NheI/XbaI* site of pcDNA3.1(+).

**Neuronal cultures.** Primary hippocampal cultures were prepared from embryonic day 16 ICR mice as described previously<sup>60</sup> with slight modifications. Briefly, hippocampi were dissected and were incubated with papain (90 units/mL, Worthington) for 20 min at 37 °C. After digestion, hippocampal cells were plated onto poly-D-lysine-coated coverslips in 24- or 12-well plates (Falcon) at a density of 20,000 cells/cm<sup>2</sup> and kept in a 5% CO<sub>2</sub> humidified incubator. At 2–4 days *in vitro* (DIV), 40 μM FUDR (Sigma) and 100 μM uridine (Sigma) were added to inhibit the growth of glial cells. One-fifth of the culture medium was replaced with fresh medium every 2–4 days. Cultures were transfected with plasmids encoding either PMCA1-SEP, SypHy, or Syntaxin-1a-SEP at 5–7 DIV using CalPhos<sup>TM</sup> mammalian transfection kit (Clontech) in accordance with a calcium phosphate transfection method which is optimized for neuronal cultures<sup>61</sup>, and were subjected to experiments at 12–14 DIV. Animals for the primary neuron cultures were treated according to our institutional guidelines for the care and use of animals (Doshisha University).

**Immunostaining.** At DIV12, neural cells were fixed with 4% (wt/vol) paraformaldehyde in phosphate buffer (Wako) for 10 min at room temperature (RT). After washing with phosphate buffered saline (PBS), the neurons were permeabilized with PBS containing 0.1% Triton X-100 for 20 min at RT, and incubated with PBS containing 10% (vol/vol) fetal bovine serum (FBS) and 0.1% Triton X-100 for 30 min at RT. The cells were incubated with rabbit polyclonal anti-GFP antiserum (1:1,000) and mouse monoclonal anti-synaptophysin antibody (1:1,000; C17.2) (both were kind gifts from Reinhard Jahn) for 1 hour at RT. The cells were rinsed three times with PBS, and further incubated with Alexa-488-conjugated anti-rabbit IgG (1:1,500; Invitrogen) and Alexa-555-conjugated anti-mouse IgG (1:1,500; Invitrogen) for 30 min at RT. After washing steps, Alexa-488 or Alexa-555 fluorescence was acquired with 470/22 nm excitation and 514/30 nm emission filters or 556- to 570-nm excitation and 600- to 650-nm emission filters, respectively.

**Live imaging.** Cells cultured on a glass coverslip were placed in a custom-made imaging chamber on a movable stage and continuously perfused with standard extracellular solution containing (in mM): 140 NaCl, 2.4 KCl, 10 HEPES, 10 glucose, 2 CaCl<sub>2</sub>, 1 MgCl<sub>2</sub>, 0.02 CNQX, and 0.025 D-APV (pH 7.4). A solution containing 50 mM NH<sub>4</sub>Cl (pH 7.4) was applied directly onto the area of interest with a combination of a fast flow exchange microperfusion device and a bulb controller, both of which were controlled by Clampex 10.2. To estimate luminal pH and surface fraction of the SEP probes, a MES-buffered solution at pH 5.5 and 50 mM NH<sub>4</sub>Cl (pH 7.4) were successively applied to cultured neurons as described previously<sup>35</sup>. Briefly, SEP fluorescence during acid quenching (F<sub>Q</sub>) and during subsequent NH<sub>4</sub>Cl application (F<sub>NH4Cl</sub>) was measured. The observed fluorescence in a given terminal is thought to be the sum of the fluorescence derived from the surface fraction of the probes (S) that experiences extracellular pH and from the vesicular fraction (1 – S) that is exposed to luminal pH (pH<sub>v</sub>). The fluorescence during the baseline (F<sub>0</sub>) and the fluorescence during F<sub>Q</sub> are expressed as

$$F_0 = S \times F_{pH\ 7.4} + (1 - S) \times F_{pHv} \quad (1)$$

$$F_Q = S \times F_{pH\ 5.5} + (1 - S) \times F_{pHv} \quad (2)$$

where F<sub>pH 5.5</sub> and F<sub>pHv</sub> are the total fluorescence values predicted when all probe molecules in a terminal are exposed to pH 5.5 and pH<sub>v</sub>, respectively. By solving Equations (1) and (2), S and F<sub>pHv</sub>/F<sub>pH 7.4</sub> were calculated as follows:

$$S = (F_0/F_{pH\ 7.4} - F_Q/F_{pH\ 7.4}) / (1 - F_{pH\ 5.5}/F_{pH\ 7.4}),$$

$$F_{pHv}/F_{pH\ 7.4} = (F_0/F_{pH\ 7.4} - S) / (1 - S).$$

According to the Henderson-Hasselbalch equation, F<sub>pH 5.5</sub>/F<sub>pH 7.4</sub> was given as follows:

$$F_{pH5.5}/F_{pH7.4} = (1/(1 + 10^{pK_a-5.5}))/((1/(1 + 10^{pK_a-7.4}))),$$

where the  $pK_a$  value of SEP estimated previously by using SypHy was 7.1<sup>53</sup>.

Finally, SV pH ( $pH_v$ ) was then calculated as follows:

$$pH_v = pK_a - \log((1 + 10^{pK_a-7.4})/F_{pH_v}/F_{pH7.4} - 1).$$

Fluorescence imaging was carried out at room temperature (~27 °C) on an inverted microscope (Olympus) equipped with a 60× (1.35 NA) oil immersion objective and 75 W Xenon lamp. Images (1024 × 1024 pixels) were acquired with a scientific CMOS camera (ORCA-Flash 4.0, Hamamatsu Photonics) with 100 ms exposure time under the control of MetaMorph software (Molecular Devices). Fluorescence of SypHy, PMCA1-SEP or Syntaxin-1a-SEP was imaged with 470/22 nm excitation and 514/30 nm emission filters.

For live imaging, images were acquired in time-lapse mode at 1 Hz under control of MetaMorph software. Field stimulation was delivered via bipolar platinum electrodes with 1 msec constant voltage pulses (50 V). A solution containing 50 mM  $NH_4Cl$  was applied at the end of recordings as described above.

**Study approval.** All experiments in this study were carried out under the approval of Doshisha University Animal Committee and Recombinant DNA Experiments Committee, and of the Institutional Animal Care and Use Committee of the RIKEN Kobe branch (approval number: QA2013-04-6). All experiments were performed in accordance with the guidelines and regulations of the respective institutions.

## Data Availability

The data that support the findings of this study are available from the corresponding authors upon reasonable request.

## References

- Edwards, R. H. The neurotransmitter cycle and quantal size. *Neuron* **55**, 835–858, <https://doi.org/10.1016/j.neuron.2007.09.001> (2007).
- Eriksen, J. *et al.* Protons Regulate Vesicular Glutamate Transporters through an Allosteric Mechanism. *Neuron* **90**, 768–780, <https://doi.org/10.1016/j.neuron.2016.03.026> (2016).
- Schenck, S., Wojcik, S. M., Brose, N. & Takamori, S. A chloride conductance in VGLUT1 underlies maximal glutamate loading into synaptic vesicles. *Nat. Neurosci.* **12**, 156–162, <https://doi.org/10.1038/nn.2248> (2009).
- Tabb, J. S., Kish, P. E., Van Dyke, R. & Ueda, T. Glutamate transport into synaptic vesicles. Roles of membrane potential, pH gradient, and intravesicular pH. *J. Biol. Chem.* **267**, 15412–15418 (1992).
- Juge, N., Muroyama, A., Hiasa, M., Omote, H. & Moriyama, Y. Vesicular inhibitory amino acid transporter is a  $Cl^-$ /gamma-aminobutyrate Co-transporter. *J. Biol. Chem.* **284**, 35073–35078, <https://doi.org/10.1074/jbc.M109.062414> (2009).
- Takamori, S. Presynaptic Molecular Determinants of Quantal Size. *Front. Synaptic Neurosci.* **8**, 2, <https://doi.org/10.3389/fnsyn.2016.00002> (2016).
- Cidon, S. & Sihra, T. S. Characterization of a  $H^+$ -ATPase in rat brain synaptic vesicles. Coupling to L-glutamate transport. *J. Biol. Chem.* **264**, 8281–8288 (1989).
- Maycox, P. R., Deckwerth, T., Hell, J. W. & Jahn, R. Glutamate uptake by brain synaptic vesicles. Energy dependence of transport and functional reconstitution in proteoliposomes. *J. Biol. Chem.* **263**, 15423–15428 (1988).
- Bellocchio, E. E., Reimer, R. J., Fremeau, R. T. Jr. & Edwards, R. H. Uptake of glutamate into synaptic vesicles by an inorganic phosphate transporter. *Science* **289**, 957–960 (2000).
- Preobraschenski, J., Zander, J. F., Suzuki, T., Ahnert-Hilger, G. & Jahn, R. Vesicular glutamate transporters use flexible anion and cation binding sites for efficient accumulation of neurotransmitter. *Neuron* **84**, 1287–1301, <https://doi.org/10.1016/j.neuron.2014.11.008> (2014).
- Juge, N. *et al.* Metabolic control of vesicular glutamate transport and release. *Neuron* **68**, 99–112, <https://doi.org/10.1016/j.neuron.2010.09.002> (2010).
- Guzman, R. E., Alekov, A. K., Filippov, M., Hegermann, J. & Fahlke, C. Involvement of ClC-3 chloride/proton exchangers in controlling glutamatergic synaptic strength in cultured hippocampal neurons. *Front. Cell. Neurosci.* **8**, 143, <https://doi.org/10.3389/fncel.2014.00143> (2014).
- Maritzen, T., Keating, D. J., Neagoe, I., Zdebek, A. A. & Jentsch, T. J. Role of the vesicular chloride transporter ClC-3 in neuroendocrine tissue. *J. Neurosci.* **28**, 10587–10598, <https://doi.org/10.1523/JNEUROSCI.3750-08.2008> (2008).
- Riazanski, V. *et al.* Presynaptic ClC-3 determines quantal size of inhibitory transmission in the hippocampus. *Nat. Neurosci.* **14**, 487–494, <https://doi.org/10.1038/nn.2775> (2011).
- Stobrawa, S. M. *et al.* Disruption of ClC-3, a chloride channel expressed on synaptic vesicles, leads to a loss of the hippocampus. *Neuron* **29**, 185–196 (2001).
- Goh, G. Y. *et al.* Presynaptic regulation of quantal size:  $K^+H^+$  exchange stimulates vesicular glutamate transport. *Nat. Neurosci.* **14**, 1285–1292, <https://doi.org/10.1038/nn.2898> (2011).
- Israel, M. *et al.* Calcium uptake by cholinergic synaptic vesicles. *J. Physiol. (Paris)* **76**, 479–485 (1980).
- Israel, M. *et al.* ATP-dependent calcium uptake by cholinergic synaptic vesicles isolated from Torpedo electric organ. *J. Membr. Biol.* **54**, 115–126 (1980).
- Michaelson, D. M., Ophir, I. & Angel, I. ATP-stimulated  $Ca^{2+}$  transport into cholinergic Torpedo synaptic vesicles. *J. Neurochem.* **35**, 116–124 (1980).
- Parducz, A. & Dunant, Y. Transient increase of calcium in synaptic vesicles after stimulation. *Neuroscience* **52**, 27–33 (1993).
- Goncalves, P. P., Meireles, S. M., Neves, P. & Vale, M. G. Synaptic vesicle  $Ca^{2+}/H^+$  antiport: dependence on the proton electrochemical gradient. *Brain Res. Mol. Brain Res.* **71**, 178–184 (1999).
- Goncalves, P. P., Meireles, S. M., Neves, P. & Vale, M. G. Distinction between  $Ca(2+)/pump$  and  $Ca(2+)/H(+)$  antiport activities in synaptic vesicles of sheep brain cortex. *Neurochem. Int.* **37**, 387–396 (2000).
- Goncalves, P. P., Meireles, S. M., Neves, P. & Vale, M. G. Methods for analysis of  $Ca(2+)/H(+)$  antiport activity in synaptic vesicles isolated from sheep brain cortex. *Brain Res. Brain Res. Prot.* **5**, 102–108 (2000).
- Neher, E. & Sakaba, T. Multiple roles of calcium ions in the regulation of neurotransmitter release. *Neuron* **59**, 861–872, <https://doi.org/10.1016/j.neuron.2008.08.019> (2008).

25. Bartholome, O. *et al.* Puzzling Out Synaptic Vesicle 2 Family Members Functions. *Front. Mol. Neurosci.* **10**, 148, <https://doi.org/10.3389/fnmol.2017.00148> (2017).
26. Janz, R., Goda, Y., Geppert, M., Missler, M. & Südhof, T. C. SV2A and SV2B function as redundant Ca<sup>2+</sup> regulators in neurotransmitter release. *Neuron* **24**, 1003–1016 (1999).
27. Wan, Q. F. *et al.* SV2 acts via presynaptic calcium to regulate neurotransmitter release. *Neuron* **66**, 884–895, <https://doi.org/10.1016/j.neuron.2010.05.010> (2010).
28. Chang, W. P. & Südhof, T. C. SV2 renders primed synaptic vesicles competent for Ca<sup>2+</sup>-induced exocytosis. *J. Neurosci.* **29**, 883–897, <https://doi.org/10.1523/JNEUROSCI.4521-08.2009> (2009).
29. Goncalves, P. P., Meireles, S. M., Neves, P. & Vale, M. G. Ionic selectivity of the Ca<sup>2+</sup>/H<sup>+</sup> antiporter in synaptic vesicles of sheep brain cortex. *Brain Res. Mol. Brain Res.* **67**, 283–291 (1999).
30. Miesenböck, G., De Angelis, D. A. & Rothman, J. E. Visualizing secretion and synaptic transmission with pH-sensitive green fluorescent proteins. *Nature* **394**, 192–195, <https://doi.org/10.1038/28190> (1998).
31. Zhang, Z., Nguyen, K. T., Barrett, E. F. & David, G. Vesicular ATPase inserted into the plasma membrane of motor terminals by exocytosis alkalinizes cytosolic pH and facilitates endocytosis. *Neuron* **68**, 1097–1108, <https://doi.org/10.1016/j.neuron.2010.11.035> (2010).
32. Hauschka, P. V. Analysis of nucleotide pools in animal cells. *Methods Cell Biol.* **7**, 361–462 (1973).
33. Plagemann, P. G. & Erbe, J. Thymidine transport by cultured Novikoff hepatoma cells and uptake by simple diffusion and relationship to incorporation into deoxyribonucleic acid. *J. Cell Biol.* **55**, 161–178 (1972).
34. Takamori, S. *et al.* Molecular anatomy of a trafficking organelle. *Cell* **127**, 831–846, <https://doi.org/10.1016/j.cell.2006.10.030> (2006).
35. Lynch, B. A. *et al.* The synaptic vesicle protein SV2A is the binding site for the antiepileptic drug levetiracetam. *Proc. Natl. Acad. Sci. USA* **101**, 9861–9866, <https://doi.org/10.1073/pnas.0308208101> (2004).
36. Lee, J. *et al.* Exploring the interaction of SV2A with racetams using homology modelling, molecular dynamics and site-directed mutagenesis. *PLoS One* **10**, e0116589, <https://doi.org/10.1371/journal.pone.0116589> (2015).
37. Michelangeli, F. & East, J. M. A diversity of SERCA Ca<sup>2+</sup> pump inhibitors. *Biochem. Soc. Trans.* **39**, 789–797, <https://doi.org/10.1042/BST0390789> (2011).
38. Cole, T. B., Wenzel, H. J., Kafer, K. E., Schwartzkroin, P. A. & Palmiter, R. D. Elimination of zinc from synaptic vesicles in the intact mouse brain by disruption of the ZnT3 gene. *Proc. Natl. Acad. Sci. USA* **96**, 1716–1721 (1999).
39. Palmiter, R. D., Cole, T. B., Quaife, C. J. & Findley, S. D. ZnT-3, a putative transporter of zinc into synaptic vesicles. *Proc. Natl. Acad. Sci. USA* **93**, 14934–14939 (1996).
40. Wenzel, H. J., Cole, T. B., Born, D. E., Schwartzkroin, P. A. & Palmiter, R. D. Ultrastructural localization of zinc transporter-3 (ZnT-3) to synaptic vesicle membranes within mossy fiber boutons in the hippocampus of mouse and monkey. *Proc. Natl. Acad. Sci. USA* **94**, 12676–12681 (1997).
41. Mitchell, S. J. & Ryan, T. A. Syntaxin-1A is excluded from recycling synaptic vesicles at nerve terminals. *J. Neurosci.* **24**, 4884–4888, <https://doi.org/10.1523/JNEUROSCI.0174-04.2004> (2004).
42. Schiavo, G. *et al.* Tetanus and botulinum-B neurotoxins block neurotransmitter release by proteolytic cleavage of synaptobrevin. *Nature* **359**, 832–835, <https://doi.org/10.1038/359832a0> (1992).
43. Thomas, R. C. The plasma membrane calcium ATPase (PMCA) of neurones is electroneutral and exchanges 2 H<sup>+</sup> for each Ca<sup>2+</sup> or Ba<sup>2+</sup> ion extruded. *J. Physiol.* **587**, 315–327, <https://doi.org/10.1113/jphysiol.2008.162453> (2009).
44. Carafoli, E. Calcium pump of the plasma membrane. *Physiol. Rev.* **71**, 129–153, <https://doi.org/10.1152/physrev.1991.71.1.129> (1991).
45. Schoch, S. *et al.* SNARE function analyzed in synaptobrevin/VAMP knockout mice. *Science* **294**, 1117–1122, <https://doi.org/10.1126/science.1064335> (2001).
46. Hicks, B. W. & Parsons, S. M. Characterization of the P-type and V-type ATPases of cholinergic synaptic vesicles and coupling of nucleotide hydrolysis to acetylcholine transport. *J. Neurochem.* **58**, 1211–1220 (1992).
47. Xie, X. S., Stone, D. K. & Racker, E. Purification of a vanadate-sensitive ATPase from clathrin-coated vesicles of bovine brain. *J. Biol. Chem.* **264**, 1710–1714 (1989).
48. Blondeau, F. *et al.* Tandem MS analysis of brain clathrin-coated vesicles reveals their critical involvement in synaptic vesicle recycling. *Proc. Natl. Acad. Sci. USA* **101**, 3833–3838, <https://doi.org/10.1073/pnas.0308186101> (2004).
49. Goncalves, P. P., Meireles, S. M., Neves, P. & Vale, M. G. Ca<sup>2+</sup> sensitivity of synaptic vesicle dopamine, gamma-aminobutyric acid, and glutamate transport systems. *Neurochem. Res.* **26**, 75–81 (2001).
50. Krebs, J. The plethora of PMCA isoforms: Alternative splicing and differential expression. *Biochim. Biophys. Acta.* **1853**, 2018–2024, <https://doi.org/10.1016/j.bbamcr.2014.12.020> (2015).
51. Madeo, M., Kovacs, A. D. & Pearce, D. A. The human synaptic vesicle protein, SV2A, functions as a galactose transporter in *Saccharomyces cerevisiae*. *J. Biol. Chem.* **289**, 33066–33071, <https://doi.org/10.1074/jbc.C114.584516> (2014).
52. Crowder, K. M. *et al.* Abnormal neurotransmission in mice lacking synaptic vesicle protein 2A (SV2A). *Proc. Natl. Acad. Sci. USA* **96**, 15268–15273 (1999).
53. Stafford, N., Wilson, C., Oceandy, D., Neyses, L. & Cartwright, E. J. The Plasma Membrane Calcium ATPases and Their Role as Major New Players in Human Disease. *Physiol. Rev.* **97**, 1089–1125, <https://doi.org/10.1152/physrev.00028.2016> (2017).
54. Hell, J. W. & Jahn, R. *Cell Biology: A laboratory Handbook* 567–574 (Academic Press, 1994).
55. Marks, P. W. & Maxfield, F. R. Preparation of solutions with free calcium concentration in the nanomolar range using 1,2-bis-(o-aminophenoxy)ethane-N,N,N',N'-tetraacetic acid. *Anal. Biochem.* **193**, 61–71 (1991).
56. Sumiyama, K., Kawakami, K. & Yagita, K. A simple and highly efficient transgenesis method in mice with the Tol2 transposon system and cytoplasmic microinjection. *Genomics* **95**, 306–311, <https://doi.org/10.1016/j.ygeno.2010.02.006> (2010).
57. Sunagawa, G. A. *et al.* Mammalian Reverse Genetics without Crossing Reveals Nr3a as a Short-Sleeper Gene. *Cell Rep.* **14**, 662–677, <https://doi.org/10.1016/j.celrep.2015.12.052> (2016).
58. Egashira, Y., Takase, M. & Takamori, S. Monitoring of vacuolar-type H<sup>+</sup> ATPase-mediated proton influx into synaptic vesicles. *J. Neurosci.* **35**, 3701–3710, <https://doi.org/10.1523/JNEUROSCI.4160-14.2015> (2015).
59. Granseth, B., Odermatt, B., Royle, S. J. & Lagnado, L. Clathrin-mediated endocytosis is the dominant mechanism of vesicle retrieval at hippocampal synapses. *Neuron* **51**, 773–786, <https://doi.org/10.1016/j.neuron.2006.08.029> (2006).
60. Egashira, Y. *et al.* Unique pH dynamics in GABAergic synaptic vesicles illuminates the mechanism and kinetics of GABA loading. *Proc. Natl. Acad. Sci. USA* **113**, 10702–10707, <https://doi.org/10.1073/pnas.1604527113> (2016).
61. Jiang, M. & Chen, G. High Ca<sup>2+</sup>-phosphate transfection efficiency in low-density neuronal cultures. *Nat. Protoc.* **1**, 695–700, <https://doi.org/10.1038/nprot.2006.86> (2006).

## Acknowledgements

We would like to thank Miki Takase and Naomi Nakai for their technical assistance, and Dr. Tetsuya Hori for critically reading the manuscript. This work was supported by grants from JSPS KAKENHI (16H04675), the JSPS Core-to-Core Program, A. Advanced Research Networks grant, and a research grant from The Uehara Memorial Foundation to S.T., and from JSPS KAKENHI (15H04408) to K.S. Finally, we would like to thank Editage ([www.editage.jp](http://www.editage.jp)) for English language editing.



### Author Contributions

Y.O., K.S. and S.T. designed experiments and wrote the manuscript. Y.O. and Y.M. performed experiments and analyzed data. Y.E. assisted with data analysis. K.S. generated all SV2-deficient mice used in this study.

### Additional Information

**Supplementary information** accompanies this paper at <https://doi.org/10.1038/s41598-019-40557-y>.

**Competing Interests:** The authors declare no competing interests.

**Publisher's note:** Springer Nature remains neutral with regard to jurisdictional claims in published maps and institutional affiliations.



**Open Access** This article is licensed under a Creative Commons Attribution 4.0 International License, which permits use, sharing, adaptation, distribution and reproduction in any medium or format, as long as you give appropriate credit to the original author(s) and the source, provide a link to the Creative Commons license, and indicate if changes were made. The images or other third party material in this article are included in the article's Creative Commons license, unless indicated otherwise in a credit line to the material. If material is not included in the article's Creative Commons license and your intended use is not permitted by statutory regulation or exceeds the permitted use, you will need to obtain permission directly from the copyright holder. To view a copy of this license, visit <http://creativecommons.org/licenses/by/4.0/>.

© The Author(s) 2019